

NUREG/CR—3532
SAND83—2098
RV
Printed November 1983

Response of Rubber Insulation Materials to Monoenergetic Electron Irradiations

W. H. Buckalew, F. J. Wyant, G. J. Lockwood

This report documents a part of the Qualification Testing Evaluation (QTE)
Program being conducted by Sandia National Laboratories

Prepared by
Sandia National Laboratories,
Albuquerque, New Mexico 87185 and Livermore, California 94550
for the United States Department of Energy
under Contract DE-AC04-76DP00789

Prepared for
U. S. NUCLEAR REGULATORY COMMISSION

NOTICE

This report was prepared as an account of work sponsored by an agency of the United States Government. Neither the United States Government nor any agency thereof, or any of their employees, makes any warranty, expressed or implied, or assumes any legal liability or responsibility for any third party's use, or the results of such use, of any information, apparatus product or process disclosed in this report, or represents that its use by such third party would not infringe privately owned rights.

Available from

GPO Sales Program

Division of Technical Information and Document Control

U.S. Nuclear Regulatory Commission

Washington, D.C. 20555

and

National Technical Information Service

Springfield, Virginia 22161

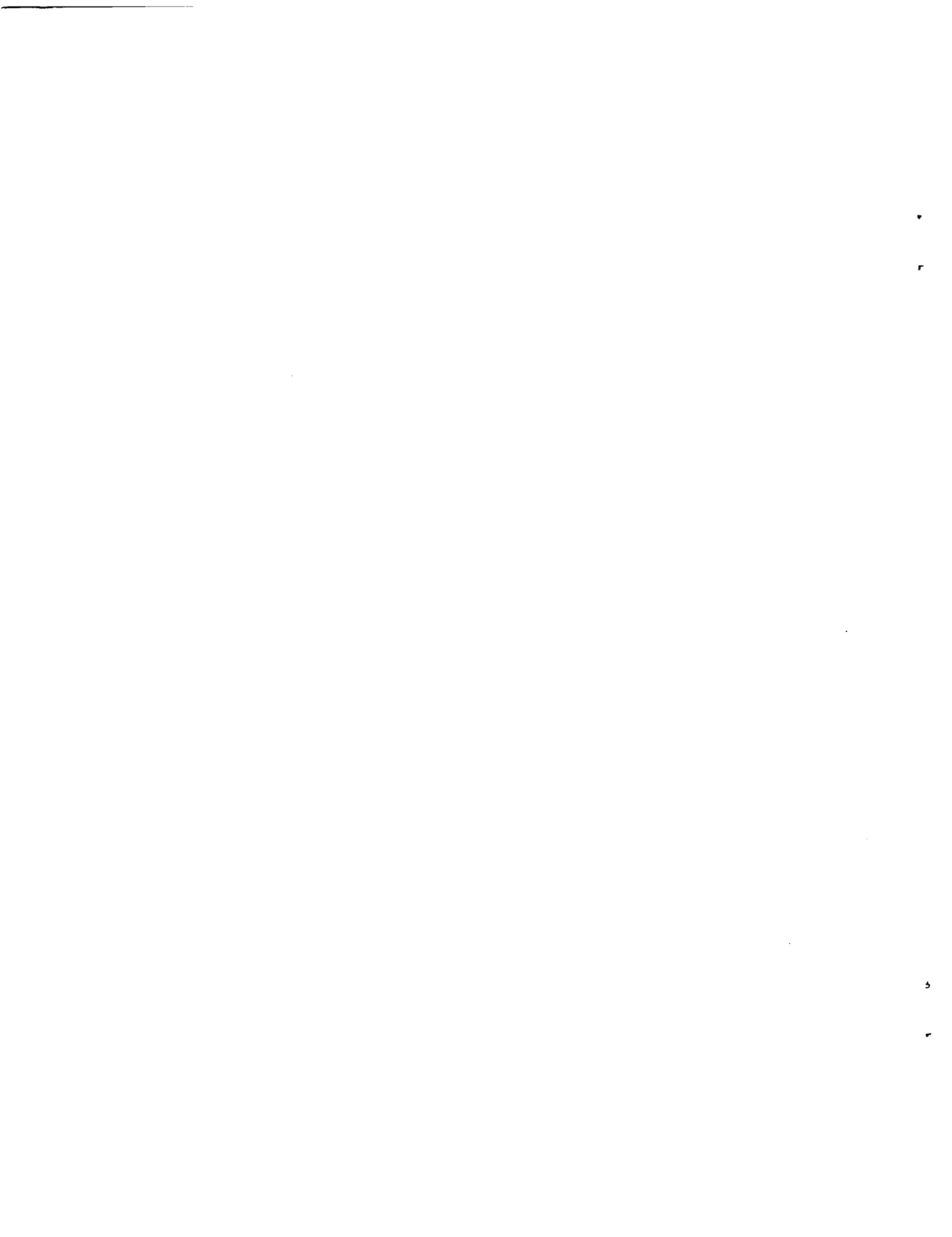
NUREG/CR-3532
SAND83-2098
RV

RESPONSE OF RUBBER INSULATION MATERIALS TO MONOENERGETIC
ELECTRON IRRADIATIONS

W. H. Buckalew, F. J. Wyant, G. J. Lockwood

Sandia National Laboratories
Albuquerque, New Mexico 87185
Operated by
Sandia Corporation
for the
U.S. Department of Energy

Prepared for the Electrical Engineering Branch
Division of Engineering Technology
Office of Nuclear Regulatory Research
U.S. Nuclear Regulatory Commission
Washington, DC 20555
Under Interagency Agreement DOE 40-550-75
NRC FIN No. A-1051



ABSTRACT

The electron charge disposition in ethylene-propylene rubber (EPR) insulation specimens irradiated with monoenergetic electrons has been investigated. Studied was charge disposition in slab and cylindrical (cable) geometries. For each geometry, charge behavior was observed as a function of environment, electron energy, and surface termination. Under certain conditions charge was accumulated and spontaneous breakdown did occur during irradiation in the vacuum environment; however, no evidence of breakdown was observed during ambient air exposures. Based on these experiments, it is concluded that electron charge buildup and breakdown is not apt to occur in EPR rubber insulation exposed to electrons from a LOCA radiation environment provided that the insulation is in contact with an ionized medium. The results can probably be applied to other organics and it appears that the LOCA beta spectra need not be precisely duplicated in insulation-radiation qualification tests.

TABLE OF CONTENTS

	<u>Page No.</u>
EXECUTIVE SUMMARY	1
1.0 INTRODUCTION	3
2.0 APPARATUS AND PROCEDURES	5
3.0 RESULTS	10
3.1 Slab Geometry	10
3.1.1 Terminated surfaces-- vacuum environment	10
3.1.2 Unterminated front surface-- vacuum environment	11
3.1.3 Terminated surfaces-- ambient environment.	13
3.1.4 Unterminated front surface-- ambient environment.	13
3.1.5 Effect of sample aluminization.	14
3.2 Cylindrical Geometry.	14
3.2.1 Ambient environment	14
3.2.2 Vacuum environment.	15
4.0 CONCLUSIONS	15
REFERENCES	17

LIST OF FIGURES

<u>Figure No.</u>		<u>Page No.</u>
1.	Reactor Containment Volume Radiation Environments.	19
2.	Gamma and Beta Particle Time-Dependent Average Energies.	20
3.	Transmission Of Recoil Electron Particle Number, Energy, And Absorbed Dose Ratio In Air	21
4.	Electron Charge Deposition In EPR From LOCA Source Electron Exposure.	22
5.	Electron Charge Deposition In EPR From Monoenergetic Electron Exposure	23
6.	Maximum Electron Beam Deflection As A Function of Raster Coil Current.	24
7.	(a) Schematic Of Experiment Orientation In Vacuum Chamber (b) Schematic Of Experiment Orientation Outside Of Vacuum Chamber.	25
8.	Schematic Of Material Sample Holder Configuration	26
9.	Schematic Of Cable Orientation In Sample Holder	27
10.	Beryllium Stopper Current Versus Faraday Cup Current	28
11.	Measured And Calculated Dose Rates Versus Beryllium Stopper Currents.	29
12.	Schematic Of Signal Measuring Configuration .	30
13.	Measured Surface Currents Versus Bias Voltage For 1.0 MeV Source Electrons.	31
14.	Measured Surface Currents Versus Bias Voltage For 0.6 MeV Source Electrons.	32

<u>Figure No.</u>		<u>Page No.</u>
15.	Measured Surface Currents Versus Back Surface Bias Voltage For 0.4 MeV Source Electrons . .	33
16.	Measured Surface Currents Versus Front Surface Bias Voltage For 0.4 MeV Source Electrons . .	34
17.	Measured Front Surface Current Versus Front Surface Bias Voltage (Expanded Scale) For 0.4 MeV Source Electrons.	35
18.	Measured Surface Currents Versus Bias Voltage For 0.2 MeV Source Electrons	36
19.	Front Surface Equilibrium Voltage As A Function Of Source Beam Energy.	37
20.	Back Surface Current As A Function Of Source Beam Energy	38
21.	EPR Front Surface Voltage Versus Time For 0.2 MeV Source Electrons.	39
22.	EPR Front Surface Voltage Versus Time For 0.45 MeV Source Electrons	40
23.	Measured Surface Currents Versus Bias Voltage For 1.0 MeV Source Electrons In Air	41
24.	Measured Surface Currents Versus Bias Voltage For 0.4 MeV Source Electrons In Air	42

LIST OF TABLES

<u>Table No.</u>		<u>Page No.</u>
1.	Incident Beam Current Partition For 1.0 MeV Source Electrons In Vacuum Environment.	43
2.	Incident Beam Current Partition For 0.2 MeV Source Electrons In Vacuum Environment.	44
3.	Comparison Of Measured And Calculated Fraction Of Incident Electrons Stopped Within EPR Volume	45
4.	Incident Beam Current Partition For 1.0 MeV Source Electrons In Ambient Air Environment. .	46
5.	Incident Beam Current Partition For 0.4 MeV Source Electrons In Ambient Air Environment . .	47

ACKNOWLEDGEMENTS

The authors would like to gratefully acknowledge the valuable technical assistance provided by S. M. Luker and L. E. Ruggles during the course of this work. In addition, E. A. Salazar supplied us the EPR formulation used, as well as the benefit of his expertise in organic material behavior.



EXECUTIVE SUMMARY

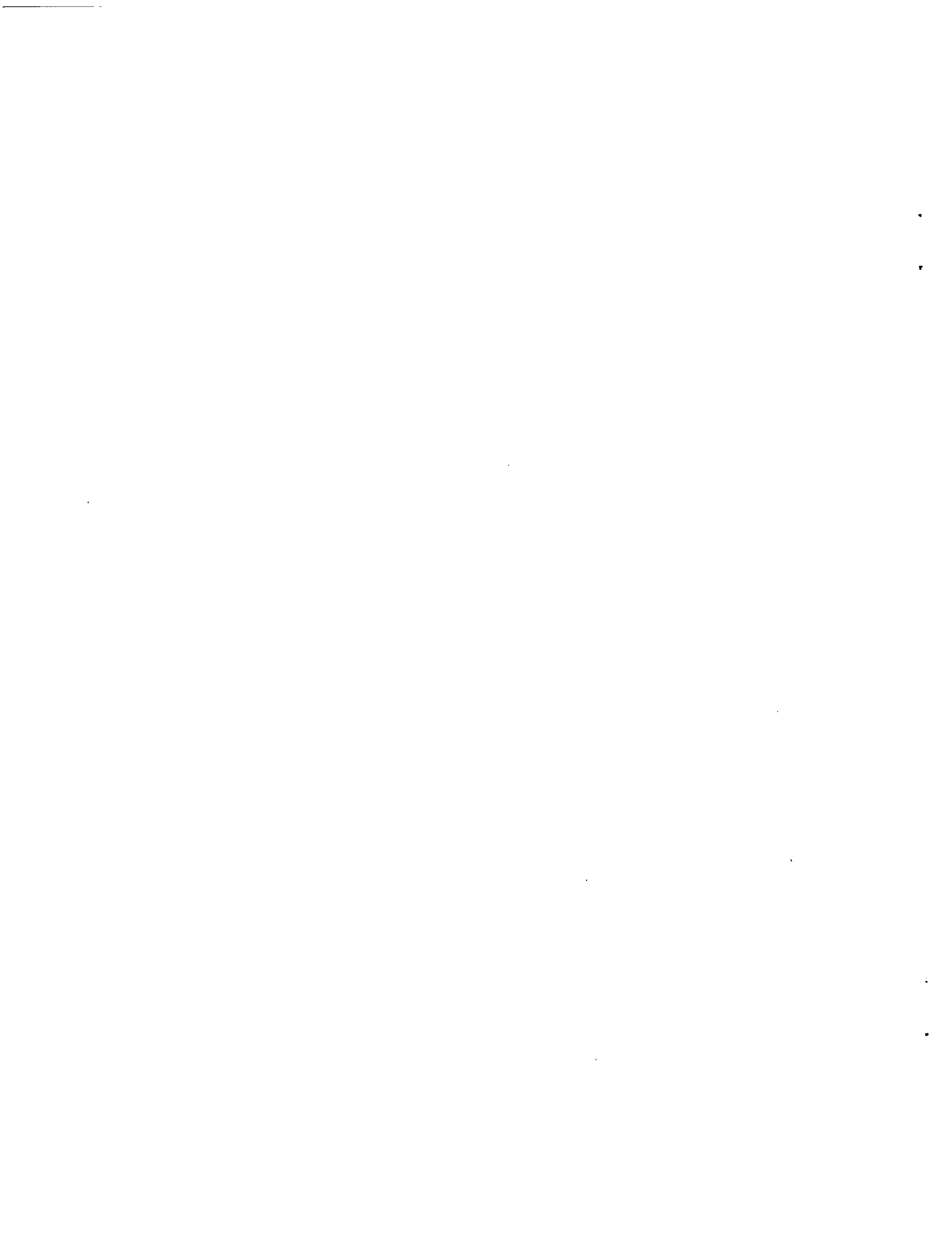
As part of a study on the adequacy of Cobalt-60 sources to simulate the radiation field accompanying a nuclear power plant loss of coolant accident (LOCA), we have investigated the electron charge disposition in ethylene-propylene rubber (EPR) insulation specimens irradiated with monoenergetic electrons.

We studied the electron charge disposition in slab samples irradiated by electrons with ranges both greater and much less than the slab thickness, under terminated and unterminated sample surface conditions. For terminated samples irradiated in a vacuum environment with penetrating electrons, no evidence of charge trapping was observed; however, we measured rapid charge buildup on unterminated surfaces of specimens irradiated with electrons with a range which was short when compared to the sample thickness. In this case the charge migrated to a terminated surface within a matter of minutes.

Similar experiments were performed with samples exposed to electron beams in an air environment. These samples exhibited no tendency to accumulate charge on unterminated surfaces--this is consistent with measured charge mobility in irradiated samples and the presence of a highly ionized interface (due to air ionization by the electrons).

Additional experiments were performed on short lengths of cables similar to those used for nuclear power plant applications. The results of this set of experiments were consistent with those obtained for the slab samples.

Based on these experiments, we have tentatively concluded that charge buildup is not likely to occur in EPR rubber insulation exposed to electrons from a LOCA radiation environment so long as the material is in contact with an ionized medium. Our results can probably be extrapolated to other organics generally, and it would appear that the LOCA beta spectra need not be exactly duplicated in simulation tests.



1.0. INTRODUCTION

Sandia National Laboratories is currently conducting the Qualification Testing Evaluation (QTE) Program [Reference 1] for the U.S. Nuclear Regulatory Commission. This program, in part, is concerned with the adequacy of gamma-radiation simulators designed to test Class 1E equipment [2] under the radiation environment characteristic of a loss of coolant accident (LOCA).

The radiation environment accompanying a LOCA is the result of the distribution of electron and photon emitting fission products throughout a reactor containment structure. It is assumed that the natural decay of these fission products will create a radiation environment with these approximate specifications [3, 4]:

- (1) An initial electron dose rate that is in excess of 10 Mrads/hr,
- (2) an ultimate integrated electron dose that is on the order of 300 to 400 Mrads,
- (3) a time-dependent energy spectrum with an average electron energy within the range of 0.2-0.8 MeV, and
- (4) a photon component with dose rates about an order of magnitude less than the electron values but with average spectral energies comparable to those from electrons.

Estimated values of the LOCA gamma and beta doses and dose rates versus time after release are plotted in Figure 1. Figure 2 shows how the in-containment gamma and beta particle average energies are expected to vary with time after release.

The distribution of fission products throughout the containment will subject Class 1E components to combined electron-photon radiation effects. For our purposes we will define LOCA radiation effects as energy and charge deposition in materials and components exposed to the radiation environment described above.

LOCA radiation effects are usually simulated using isotopic sources, generally Cobalt-60. In contrast to a LOCA radiation environment, Cobalt-60 decays by the emission of a 0.32 MeV beta particle, and two photons with energies of 1.17 and 1.33 MeV. Because of its low energy, the beta particle is (for all practical purposes) absorbed within the source. From the standpoint of energy deposition, Co-60 irradiators can adequately simulate the LOCA photon component in all aspects [5] (i.e., total energy deposition, energy deposition profile, and deposition rate);

however, electron effects are in some instances less adequately simulated and electron charge deposition probably not at all.

Cobalt-60 photon transport through air can result in the development of a sizeable electron component. Photon transport in air was calculated using the coupled electron-photon transport code, TIGER [6], to demonstrate the buildup of the recoil electron spectrum. The results of this calculation are shown in Figure 3, where we have plotted transmitted electron number (charge) and energy, and the absorbed electron/photon dose ratio as a function of air slab thickness. We note, (Figure 3), simulation of a LOCA electron radiation environment by this technique is probably not feasible when the LOCA electron/photon dose ratio and the photon mean free path in air are considered; i.e., the requirement of megacurie sources and an irradiation cell with dimensions comparable to the recoil electron mean free path in air (about 3 meters). In view of the above, we chose to investigate the electron effects with an electron accelerator capable of providing electron energies and dose rates comparable to those values associated with the LOCA beta spectra (0.2 to 1.0 MeV at dose rates between 1.0 to 40 Mrads/hr).

Specifically, we are concerned with the effects of electron bombardment on the performance of organic cable insulations used in reactor applications. Since there is a continuum of LOCA electron spectra, we restricted this study to the effects of the softest (4-day) and hardest (1-minute) spectra expected [3, 4, 5].

In Figure 4 we present the results of TIGER calculations, which predict the electron charge distribution for the transport of these two spectra through a representative thickness of a typical ethylene-propylene rubber (EPR) formulation [7]. We note the salient differences in the electron distributions resulting from the two incident spectra. In one instance (4-day spectrum) we observe that the distribution is concentrated in the vicinity of the material front surface, in the other case we see that the fraction of electrons deposited in the first 0.05 cm of material is about a factor of 3 less. The code used for this calculation predicts the electron deposition, but not ultimate disposition; i.e., trapping, mobility, etc. If the effects of electron bombardment on the electrical performance of cable dielectrics is to be predicted, then the ultimate disposition of deposited electrons must be known. In other words, for an extended irradiation with energetic electrons, is a charge buildup observed or does the charge find its way to ground? Similar questions arise regarding the electron distribution associated with low energy electron transport.

We calculated the electron charge deposition in dielectric samples irradiated with monoenergetic electrons, whose ranges were both less than and greater than the sample thickness. For comparison with the spectral results (Figure 4), we include Figure 5, showing some representative electron distributions in EPR slabs for several monoenergetic electron source energies. As can be seen, the electron deposition profiles calculated for both LOCA beta spectra, in Figure 4, are effectively bounded by a superposition of the electron beam deposition profiles calculated for the three monoenergetic beams (Figure 5).

Experiments were performed by exposing typical EPR materials (slab and cylindrical geometries) to monoenergetic electrons (0.2 to 1.0 MeV) in vacuum and ambient air environments. For all incident electron energies (in vacuum), we studied charge mobility for both voltage biased and unbiased conditions and the effects of surface terminations on charge buildup in the material. Similar experiments, but with less extensive energy ranges, were performed on the same materials and geometries with the electron beam extracted into ambient air. By observing surface voltages and the partition of the accelerator total beam current, we were able to deduce the response of selected cable insulation materials to LOCA-like electron radiation fields; i.e., charge accumulation and surface potential buildup.

2.0. APPARATUS AND PROCEDURES

We used a Pelletron* electron accelerator to produce the electron radiation fields used in our experiments. The accelerator is variable in electron energy and beam current. The electron energy range is between 0.025 and 1.2 MeV, and beam current is adjustable up to a maximum of 34 microamps. Uncertainties in the machine parameters (voltage regulation and ripple) were carefully determined such that the electron beam energy is known to within approximately 0.5% [8]. Total beam current is determined with an "in-line" Faraday Cup, whose output is monitored with an electrometer. Most applications of this accelerator (dose-depth determinations, transport code verifications, etc.) [9, 10] require a tightly confined (i.e., small diameter) electron beam incident on the target. Our application, on the other hand, requires a diffuse beam pattern. Accordingly, we designed a magnetic beam deflector system that can produce rastered beams resulting in uniform rectangular patterns with dimensions on the order of 15 centimeters. Pre-experiment diagnostics allowed accurate prediction of beam pattern size based on deflector magnet coil current, current frequency, and electron beam energy. An example of these

*Manufactured by National Electrostatics Corporation, Middleton, WI.

diagnostic data is presented in Figure 6, which depicts electron deflection data as a function of magnet coil current for two current frequencies. (A companion report [11], describing the capabilities of the new accelerator-raster system and providing all of the diagnostic results, will soon be published).

The beam deflection assembly is attached, in tandem, to the Faraday Cup back flange. Integral with the accelerator is a 1.2 meter (diameter) stainless steel vacuum chamber, equipped with several fixtures to accommodate in-vacuum experiments. In Figure 7a the orientation of the accelerator (electron beam) column, vacuum chamber, and the various components within the vacuum chamber is shown. The electron beam is extracted from the accelerator column and steered into the vacuum chamber through the Faraday Cup mounted on the chamber interior wall. A movable plate on the Faraday Cup permits either monitoring of the total beam current (closed) or transmission of the beam into the tank (open). Mounted on the Faraday Cup back surface is the beam deflector (raster) unit. For in-vacuum irradiations, a target mounting fixture (including a high-voltage feedthrough insulator) is positioned near the vacuum chamber wall and diametrically opposite to the Faraday Cup. This configuration allows maximum raster-target separation and hence maximum electron beam pattern size.

For irradiations under ambient (air) conditions, the experiment package is moved in toto outside the vacuum chamber and positioned behind the feedthrough insulator port. The following modifications complete the transition: The high-voltage feedthrough insulator is replaced with a 0.003-cm thick mylar window and, in order to define the electron beam prior to exit from the vacuum tank, an additional mask is placed just ahead of the mylar retaining assembly in the port. In Figure 7b, the experiment package orientation for ambient air irradiations is shown with respect to the vacuum chamber.

Figure 8 shows the experiment (target) package configuration used with slab geometry. It is essentially a three-element unit. The lead element is an aluminum mask whose purpose is to define the dimensions, or pattern, of the electron beam incident on the target surface. Additionally, the mask, whose thickness is infinite to the most energetic source electron, assures beam spatial uniformity across the front surface of the sample in that the incident beam pattern is sized so that it is always larger than the mask orifice. This condition assures that the non-uniform electron distribution near the raster periphery, due to the scanning magnet inductance, is masked from the target. Adjacent to the mask element is the sample holder. The holder, positioned approximately 1.3 centimeters behind the mask, is a two-piece aluminum frame. This frame

allows rigid clamping of the test specimen samples. The frame halves are secured with nylon screws so that the pieces are electrically isolated and may serve as signal electrodes. The entire frame and secured target are suspended in "free space" via the frame support/signal bar. For in-vacuum experiments the frame support fixture is connected to a high-voltage feed-through insulator, located in a flanged port on the vacuum chamber wall. Positioned 1.3 centimeters behind the sample holder is an infinitely thick (to electrons) element consisting of a 0.2-cm thick beryllium plate in intimate contact with a 0.3-cm thick aluminum plate. This stopper plate assembly allows absorption of all electrons traversing the sample and the beryllium component of the stopper assembly assures minimum reflection of the transmitted electrons back into the test sample's rear surface.

For the cylindrical configuration, the standard experimental package was used to hold cable specimens during irradiation. The cables were of sufficient length so that signal terminations could be made outside the radiation environment. Orientation of the cables in the experiment fixture is shown in Figure 9.

The two material sample configurations were studied--a slab geometry and a cylindrical configuration. The slab geometry samples are 0.15-cm thick generic ethylene-propylene rubber sheets [7] comparable to EPR-type insulations currently used in nuclear plant cable applications. Both surfaces of the test specimens are coated with a five-micron layer of vacuum deposited aluminum. The aluminum coating allows application of bias voltage and/or detection of surface currents/potentials. In some applications with terminated surfaces and either zero or low applied voltages, samples with complete coating on both surfaces were used. We assured by experiment that no alternate electrical paths developed across the small sample dimension. In charge buildup experiments involving unterminated surfaces, we increased the surface-to-volume breakdown path ratio by removing a portion of the aluminum coating from one surface. This procedure reduced the coated area to about 7.5 square centimeters, as opposed to a total, single-surface, coated area of 58 square centimeters. Electrical contact to the smaller aluminum coating was made by cementing a #20 varnished copper wire to it. The modified sample geometry, with termination lead, is shown in Figure 8. Contact to the other (fully-coated) surface was made through the sample retaining frame. In applications using samples with reduced surface coating, the fully-coated surface was oriented toward the electron beam. A mask with an orifice smaller than the reduced coating dimension was always used in these applications.

The cylindrical configurations are representative of cables used in nuclear plant applications. Both sample types have 0.08-cm ethylene-propylene rubber insulation, one encased in a 0.04-cm thick chlorosulfonated polyethylene jacket and the other in a 0.04-cm thick neoprene jacket. The conductor is a 0.2-cm diameter tinned copper wire.

Extensive dosimetry measurements were made prior to the actual experiments. The electron beam pattern size and uniformity were characterized as a function of raster parameters using 0.005-cm thick dye-loaded nylon and polychlorostyrene thin-film dosimeters. Film calibration (response) to ionizing radiation was established by exposing equilibrated films to a Cobalt-60 gamma source, positioned in a dry (air) cell. Cobalt-60 dose and dose rates were measured using an NBS traceable air ionization chamber (Victoreen 550 Radacon III). Dosimeter response measured was the growth of absorption peaks in the film, as a function of absorbed energy. The absorption data was measured with a recording microdensitometer. In addition to beam uniformity measurements, a correlation between total beam current and specimen dose was established. For several beam energies and currents, we used the dye-loaded plastics to measure the resultant doses in the sample holder frame. The corresponding beam currents detected by the beryllium stopper were then used to estimate the doses using calculated current-to-dose conversion factors [11] appropriate for the geometry. The results of the measurements and calculations are presented in Figures 10 and 11. Figure 10 shows the relationship between Faraday Cup and beryllium stopper currents for each beam energy. The relationship between dose rates, as measured with the films and calculated on the basis of stopper currents, are given in Figure 11. The fall-off in dosimeter response at the higher dose rates shown in Figure 11 is attributed to oxygen depletion in the dosimetry films during these irradiations, which were made in a vacuum environment. For confirmation, we compared the response of dosimeters irradiated, to identical doses, in vacuum and ambient air environments. The indicated dose for the dosimeter irradiated in the vacuum environment was less than indicated dose for the dosimeter exposed in the air environment. Further, the electron dose measurements in air environments agreed with doses calculated on the basis of beryllium stopper currents.

Our study of electron effects in dielectrics has consisted, thus far, of examining electron charge mobility and surface potential (voltage) buildup in slab and cylindrical geometries for both vacuum and ambient (air) environments. Since reactor accident radiation environments can be represented as quasi steady state, all sample irradiations were in a steady state radiation field. We studied charge mobility by observing surface and transmitted electron currents using slab geometry samples with terminated surfaces. Figure 12 presents a schematic

of the instrumentation used for the charge mobility measurements. The E-i's are electrometers used to detect and measure mask, surface, and stopper currents. Mask, back surface, and stopper current records are obtained with the R-i chart recorders. Back surface bias is applied by a continuously variable bipolar DC power supply in the range of ± 600 VDC. In anticipation of possible charge trapping and voltage break-down, we included the capability of capacitive coupling of an oscilloscope to the sample back surface. Charge mobility, with both sample surfaces terminated, was such that no evidence of charge breakdown were observed with the oscilloscope. For mobility measurements we observed the I-i currents for bias voltages in the range of ± 600 VDC. Knowing the Faraday Cup current, we were able to accurately estimate the total current incident on the experiment package. Conservation of steady state currents incident on the package, coupled with the absence of high-frequency transients was taken as evidence of charge mobility within the material. For the surface potential buildup experiments, we replaced E-2 with an electrostatic voltmeter and shunted the bipolar power supply; the sample back surface was then terminated to ground through the electrometer, E-3. Front surface voltage buildup was restricted to 12.5 kV--the voltage rating on the high voltage feedthrough insulator. For the front surface potential measurements, the sample was irradiated until either breakdown occurred or a steady state surface potential was established.

Charge mobility measurements on the cylindrical specimens were more limited. The samples, representative of materials used in nuclear plant installations, have no conductive coating on the outer surface, thus barring front surface termination. In this instance, charge mobility determination was restricted to monitoring the central conductor current. For energetic electrons, with a range greater than material thickness, we assumed establishment of a steady current as a measure of charge mobility. Front surface potential buildup and discharge, on the other hand, was assumed--independent of electron energy--if sporadic current spikes were observed on the central conductor. In addition, because of the capacitive coupling between the experiment package elements, spontaneous loss of charge (break-down) in the test sample always resulted in induced spikes being superimposed on the beryllium stopper current.

Ambient-environment experiments were similar to, but somewhat abbreviated versions of, those performed in vacuum; i.e., these irradiations were done at 0.4 and 1.0 MeV only.

3.0. RESULTS

3.1 Slab Geometry

3.1.1 Terminated surfaces--vacuum environment

Electron disposition in 7.6 by 7.6 by 0.15-cm generic EPR rubber insulation samples was measured as a function of incident electron energy and applied surface bias voltage. The circuit shown in Figure 12, but without the oscilloscope, was used to measure current disposition. Pressure in the vacuum chamber was in the sub-millitorr range during all of the experiments. Monoenergetic electrons with energies of 0.2, 0.4, 0.6, 0.8, and 1.0 MeV were used in these determinations. Thus the range of bombarding particles varied from much less to greater than the sample thickness. The electron beam pattern was approximately 9 by 9 cm square. An aluminum mask reduced the beam pattern, incident onto the sample, to a 6.4 by 6.4 cm square area. Depending on the experiment, the radiation dose rate delivered to the sample front face was between 1.0 and 40 Mrad(air)/hr. Bias voltage was applied to the sample rear surface in all instances except for one 0.4 MeV exposure, where the bias was applied to the front surface. Each irradiation was of sufficient duration to assure that steady state conditions had been achieved.

Table 1 gives a tabulation of the 1.0 MeV data. The mask data (Column 1) have been corrected [10] for electron backscatter. As may be observed from the last column, the ratio of partitioned current to incident current, the incident beam current is well accounted for. Similar data were obtained for the other, lower energy, irradiations; i.e., a reasonable accounting for the total current disposition.

Figure 13 is a graph of the 1.0 MeV data. The surface currents have been normalized on the basis of the incident (Faraday Cup) current. Of interest is the indication of charge mobility within the sample due to the presence of a biasing voltage. Some changes in the observed back surface current are, no doubt, influenced by the effect of the back surface bias voltage on electron reflection from the beryllium stopper.

The 0.6 MeV data are shown in Figure 14. Since the 0.6 MeV electron range is also greater than the sample thickness, the

data are similar to those observed for the 1.0 MeV irradiations. Of note, however, is the increased normalized surface currents compared to their 1.0 MeV counterparts. This observation is consistent with calculated results which predict increasing charge deposition with decreasing electron energy.

Figures 15, 16, and 17 show plots of the 0.4 MeV irradiation data. Since 0.4 MeV electrons have a range less than the material thickness, we note the zero back surface current. Note also the ineffectiveness of the back surface bias. The effectiveness of the front surface (negative) bias in preventing secondary electrons from returning to the material front surface is demonstrated in Figure 16; also observe the increase in front surface current, due to collected secondaries when the applied bias voltage is increased in the positive direction. (This effect is dramatically shown on the expanded surface current scale in Figure 17). Some of the observed increase in front surface current might be due to the collection of low energy mask recoil electrons drawn through the mask aperture.

The data for the 0.2 MeV irradiations are plotted in Figure 18. These data are consistent with the 0.4 MeV back surface biased data. Table 2 gives the current partition data for the 0.2 MeV irradiation. This table is identical in format to Table 1. Of interest in this tabulation is the zero back surface and beryllium stopper currents.

Since, in all cases, both surfaces were terminated (to ground) through instruments with internal impedance on the order of one megohm, surface potentials achieved were on the order of volts.

Table 3 is a tabulation of the charge disposition data for each (energy) irradiation. The sum of normalized front surface and back surface currents versus beam energy is tabulated. The sums of the measured results are compared to the calculated total (normalized) number of electrons stopped within the EPR material for the incident energies. Agreement between measured and calculated values may be seen in the last column. Note that this table is for terminated surface cases only, but this table and the data in Tables 1 and 2 taken together show that electrons stopped in the EPR are mobile enough (to go to ground) such that no charge trapping occurs.

3.1.2 Unterminated front surface--vacuum environment

Front surface charge/potential buildup in the slab geometry was studied with 0.2, 0.4, 0.45, 0.6, 0.8, and 1.0 MeV electron beam energies. The circuit shown in Figure 12 was used with

the electrometer E-2 and the bias supply removed. An electrostatic voltmeter replaced the electrometer E-2. For these experiments, the back surface aluminum coating was reduced to a 2.9 by 2.9 cm square and, in addition, the mask orifice was reduced to a 2.5-cm diameter circular opening. In line with the reduction in the mask orifice, the beam pattern was reduced to 4.8 by 4.4 centimeters. Because of the considerable capacitance in the total system, these irradiations were performed at dose rates in the range of 10 to 40 Mrad(air)/hr. Since the high-voltage components, the feedthrough insulator and electrostatic voltmeter, were rated at 12.5 kilovolts, our experimental strategy was to irradiate the samples until an equilibrium front surface voltage was achieved or breakdown occurred, unless it was evident that the front surface potential would exceed the equipment rating; in that case the experiment would be terminated as the equipment voltage rating was reached.

Using these guidelines, we studied charge buildup accompanying 1.0 MeV irradiation at dose rates of 10, 20, and 30 Mrad(air)/hr. No evidence of dielectric breakdown was observed and only modest increases in front surface voltage accompanied the increases in dose rate. Samples were then irradiated with 0.2, 0.4, 0.45, 0.6, and 0.8 MeV electrons. Sample behavior was not always consistent. Charging times for electrons with ranges short compared to sample thickness varied from tens of seconds to the order of tens of minutes. These anomalies may have been, in part, due to the high-voltage system. For example, upon reaching a front surface voltage equilibrium we were unable to account for the total incident current disposition.

The front surface voltage buildup results are presented in Figures 19 and 20. In Figure 19, front surface equilibrium voltage is plotted as a function of electron energy. The data at 0.2 MeV are probably dependent on the "standoff" capabilities of our system. Figure 20 shows the observed back surface current associated with the same beam energies. The decrease in observed back surface current with increasing electron energy is due to the increased range of the more energetic particles.

In general, we observed a voltage buildup on the unterminated (from ground) surface. Additionally, for irradiations with electrons with a range greater than the sample thickness, breakdown did not occur. In all other cases, breakdown occurred somewhere in the system.

During the course of these experiments, we observed evidence of radiation damage. Since we intend to investigate this possibility further, we present the data without elaboration. These data were obtained as explained earlier. Figure 21 shows a plot of the time history of the front surface voltage of a

sample irradiated with 0.2 MeV electrons, electrons with a range much less than the sample thickness. We observed a front surface equilibrium voltage of approximately 12 kilo-volts. The discontinuity indicates cut-off of the electron beam with subsequent decay of the accumulated charge on the sample. Following a short irradiation (approximately five minutes) with 1.0 MeV electrons we repeated the irradiation (at 0.2 MeV) and observed an equilibrium voltage on the order of one half the pre-1.0 MeV irradiation value. Similar data for 0.45 MeV electrons, range approximately equal to the sample thickness, are presented in Figure 22.

3.1.3 Terminated surfaces--ambient environment

For these experiments, the electron beam was extracted through a 0.003-cm mylar window and onto the standard experiment package (shown in Figure 8). An additional mask was placed just ahead of the mylar. Instrumentation was as depicted in Figure 12. For these experiments the small electron beam pattern and 2.5-cm mask aperture were used. Exposures were at 30 Mrad(air)/hr with 0.4 and 1.0 MeV electron beam energies. Surface currents as a function of back surface bias voltage were again measured.

The 1.0 MeV data are presented in Table 4. The data presented are the same as in Table 1 except for the addition of a second mask current (IM2). The point of interest in this tabulation is the presence of the large ionization currents existing in the gaps between the experiment fixture elements and detected by the enhanced front surface, back surface, and beryllium stopper currents. The magnitude of these currents was sufficient to mask the primary surface currents. Similar data were obtained for the 0.4 MeV irradiation, and are shown in Table 5.

Figures 23 and 24 are plots of the currents measured by the front and back surface electrometers as a function of bias voltage for the 1.0 and 0.4 MeV irradiations, respectively. As may be observed in both cases, the onset of voltage saturation of the air-generated ion current is not indicated (i.e., no tendency for the back surface current to reach a limiting value with increasing back surface bias voltage).

3.1.4 Unterminated front surface--ambient environment

Breakdown determinations were made with 1.0 and 0.4 MeV electron energies at approximately 24 Mrad(air)/hr for each energy. During the 1.0 MeV beam energy irradiation, the front surface voltage was observed for approximately five minutes. During this exposure, the front surface reached an equilibrium voltage of 100 volts within 30 seconds and the back surface

current remained constant at 0.06 microamps. No current spikes were superimposed on either the back surface or beryllium stopper current traces. This experiment was repeated with a 0.4 MeV beam. Front surface voltage equilibrium was again achieved in 30 seconds, but at 200 volts. The back surface current remained at zero throughout the irradiation, with no evidence of current discharge transients. Following these two irradiations, the sample was again exposed in the vacuum environment to the 0.4 MeV energy beam to confirm that the sample could maintain a front surface (high) potential. An equilibrium front surface voltage of 2.4 kV was obtained within one minute.

3.1.5 Effect of sample aluminization

The effects of sample aluminization on charge mobility and surface potential buildup were examined in both vacuum and ambient environments. For these experiments, the aluminum coating was removed from the entire front surface of the samples. Potential buildup and breakdown were monitored by observing back surface current disturbances and their induced effects on the beryllium stopper currents. In addition, an oscilloscope was capacitively coupled to the sample back surface.

No effects were observed that could be attributed to the aluminization. A thirty minute ambient exposure to the 0.4 MeV beam, at 25 Mrad(air)/hr produced no evidence of surface buildup and/or breakdown. In the vacuum environment and at low beam energy exposures, however, breakdown occurred in seconds--indicative of the magnitude of the external (measuring) circuit capacitance.

3.2 Cylindrical Geometry

Experiments on the cylindrical geometry were similar to those performed on the slab geometry, except that studies of charge mobility and surface potential buildup were restricted to beam energies of 0.4 and 1.0 MeV. Surface potential buildup and discharge were detected by observing transients appearing on the central conductor current trace and induced transients appearing on the beryllium stopper.

3.2.1 Ambient environment

The two cylindrical, 23-cm long, samples were exposed to the 0.4 MeV beam energy at a dose rate of 25 Mrad(air)/hr for 10 minutes. Central conductor and beryllium currents were observed throughout the exposure. Central conductor currents were zero and free of any transient spikes. The beryllium stopper current was constant at 0.19 microamps and exhibited no imposed induced transients.

3.2.2 Vacuum environment

These two samples were exposed to both the 1.0 and 0.4 MeV beam environments at a dose rate of 30 Mrad(air)/hr. The 1.0 MeV beam energy was performed first. For this exposure, central conductor currents were steady state with no evidence of current breakdown pulses. In addition, the beryllium stopper current trace was also steady state with no evidence of induced current spikes. Cable behavior during the 0.4 MeV beam irradiation was markedly different. Both cylindrical central conductor currents were zero, consistent with the electron range compared to sample thickness. Superimposed on the zero current traces were current spikes indicative of current discharge to the central conductors. These spikes appeared within 10 seconds of the onset of irradiation. The accompanying beryllium stopper current trace detected these discharges via induced transient current spikes.

4.0. CONCLUSIONS

We investigated the response of different EPR-type rubber insulation materials to electron environments with electron ranges both less than and greater than the sample thickness, and for both vacuum and ambient environments.

Results from the vacuum environment experiments suggest that charge trapping, if present, is insignificant. For electrons with ranges short compared to sample thickness, a surface buildup and discharge will occur for an unterminated surface; however, if the surface is terminated, charge flow will inhibit buildup and breakdown. For energetic electrons, buildup will not occur regardless of termination.

In ambient environments, air ionization produced by the electrons is of sufficient magnitude to neutralize any surface charge accumulation by the irradiated sample regardless of the incident electron energy; i.e., electron range less than or greater than the sample thickness. These results were observed to be independent of the sample geometry--slab or cylindrical.

Since the experiments were designed to approximate the reactor loss of coolant accident (LOCA) electron radiation field, we believe that these data may be applied to predict the disposition of LOCA electrons incident on organic-insulated electrical cables and the response of these insulations to the electrons. Thus we conclude that so long as "EPR-like" insulated cables are in contact with an ionizable gaseous medium, charge buildup and discharge in the cable rubber insulation will not occur as the result of exposure to the LOCA electron radiation environment.

We observed radiation damage to the insulation material after short exposures to 1.0 MeV electrons, in vacuum, with a lowering of ultimate achievable surface potential buildup. This lowering of ultimate surface potential was also accompanied by an inability to account for the total incident electron beam current. This damage phenomenon needs further study as does the combined electron-photon effects on charge transport, mobility, and ultimate surface voltage buildup.

REFERENCES

1. L. L. Bonzon, et al., "An Overview of Equipment Survivability Studies at Sandia National Laboratories (SNL)," SAND83-0759C, Sandia National Laboratories, Presented at the International Meeting on Light-Water Reactor Severe Accident Evaluation Conference, Cambridge, MA, August 28-September 1, 1983.
2. IEEE Standard for Qualifying Class 1E Equipment for Nuclear Power Generating Stations, IEEE Std. 323-1974, The Institute of Electrical and Electronic Engineers, Inc., 1974.
3. L. L. Bonzon, "Radiation Signature Following the Hypothesized LOCA," SAND76-0740, NUREG76-6521, Sandia National Laboratories, Rev. October 1977.
4. L. L. Bonzon, et al., "Definition of Loss-of-Coolant-Accident Radiation Source: Summary and Conclusions," SAND78-0091, Sandia National Laboratories, May, 1978.
5. L. L. Bonzon and W. H. Buckalew, "Evaluation of Simulator Adequacy for the Radiation Qualification of Safety-Related Equipment," SAND79 1787, NUREG/CR-1184, Sandia National Laboratories, January, 1980.
6. J. A. Halbleib, Sr. and W. H. Vandevender, Nucl. Sci. Eng., 57, 94(1975).
7. E. A. Salazar, D. A. Bouchard, and D. T. Furgal, "Aging With Respect to Flammability and Other Properties in Fire-Retarded Ethylene Propylene Rubber and Chlorosulfonated Polyethylene," SAND81-1906, NUREG/CR-2314, Sandia National Laboratories, March, 1982.
8. G. H. Miller and G. J. Lockwood, IEEE Trans. Nucl. Sci., NS-22, 1072(1975).
9. G. J. Lockwood, L. E. Ruggles, G. H. Miller, and J. A. Halbleib, "Calorimetric Measurements of Electron Energy Deposition in Extended Media - Theory vs Experiment," SAND79-0414, Sandia National Laboratories, January, 1980.

10. G. J. Lockwood, L. E. Ruggles, G. H. Miller, and J. A. Halbleib, "Electron Energy and Charge Albedos - Calorimetric Measurements vs Monte-Carlo Theory," SAND80-1968, Sandia National Laboratories, November, 1981.
11. W. H. Buckalew, G. J. Lockwood, and F. J. Wyant, "Capabilities and Diagnostics of the Sandia Pelletron-Raster System," (Unpublished), 1983.

Containment Volume Radiation Environments

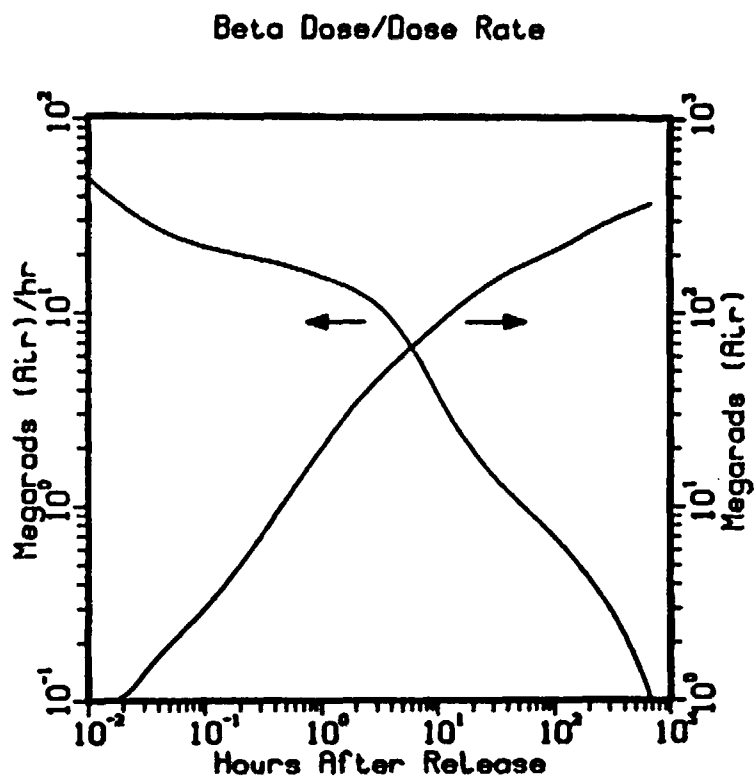
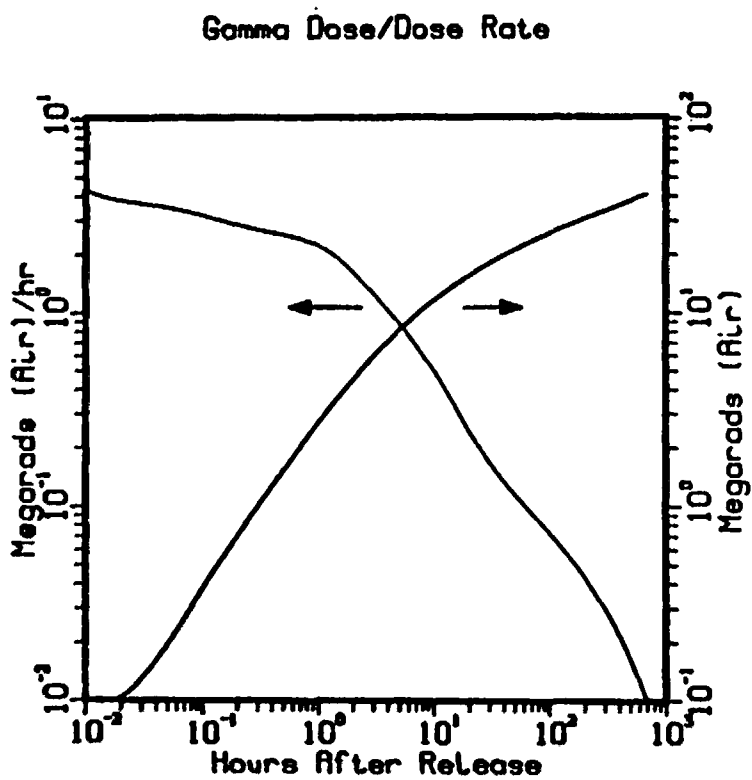


Figure 1. Reactor Containment Volume Radiation Environments.

Average Gamma-Ray and Beta Particle Energy in Air versus Reactor Cooling Time

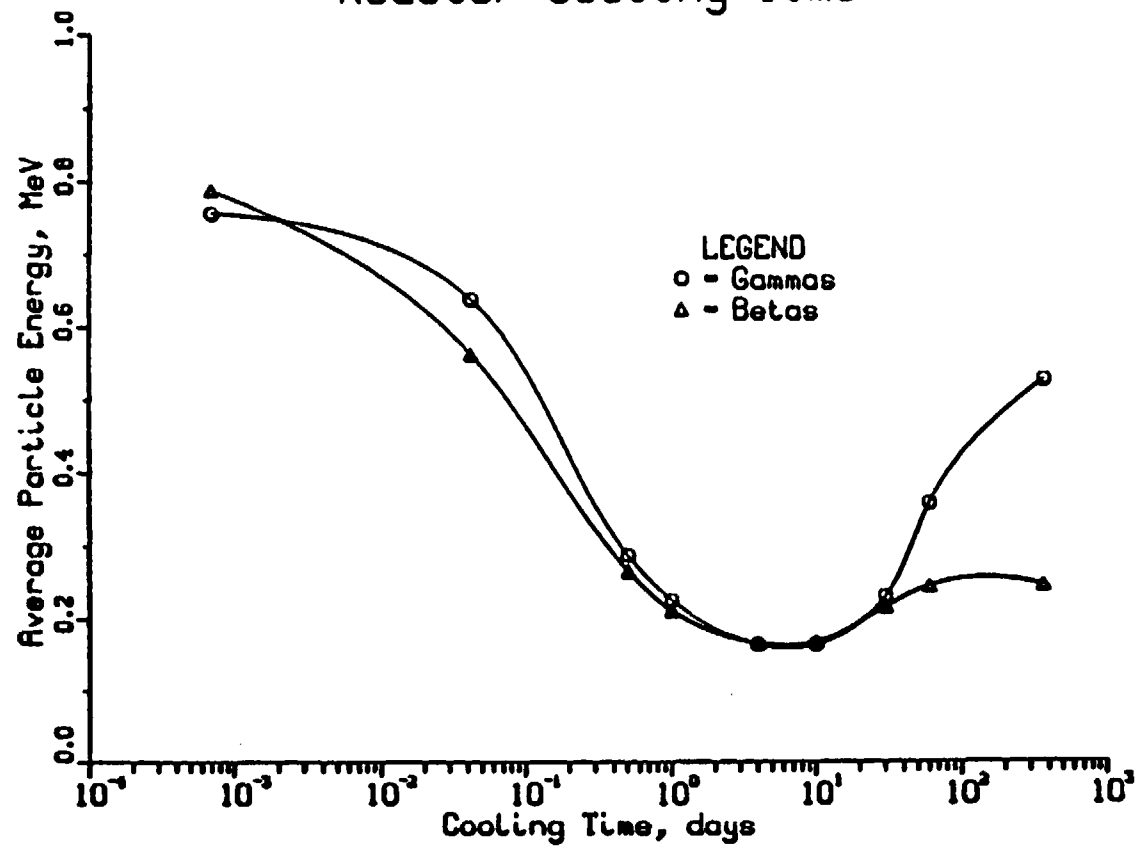


Figure 2. Gamma and Beta Particle Time-Dependent Average Energies.

Electron Number-Energy Transmission versus Slab Thickness 1.25 MeV Photons incident on STP Air Slabs

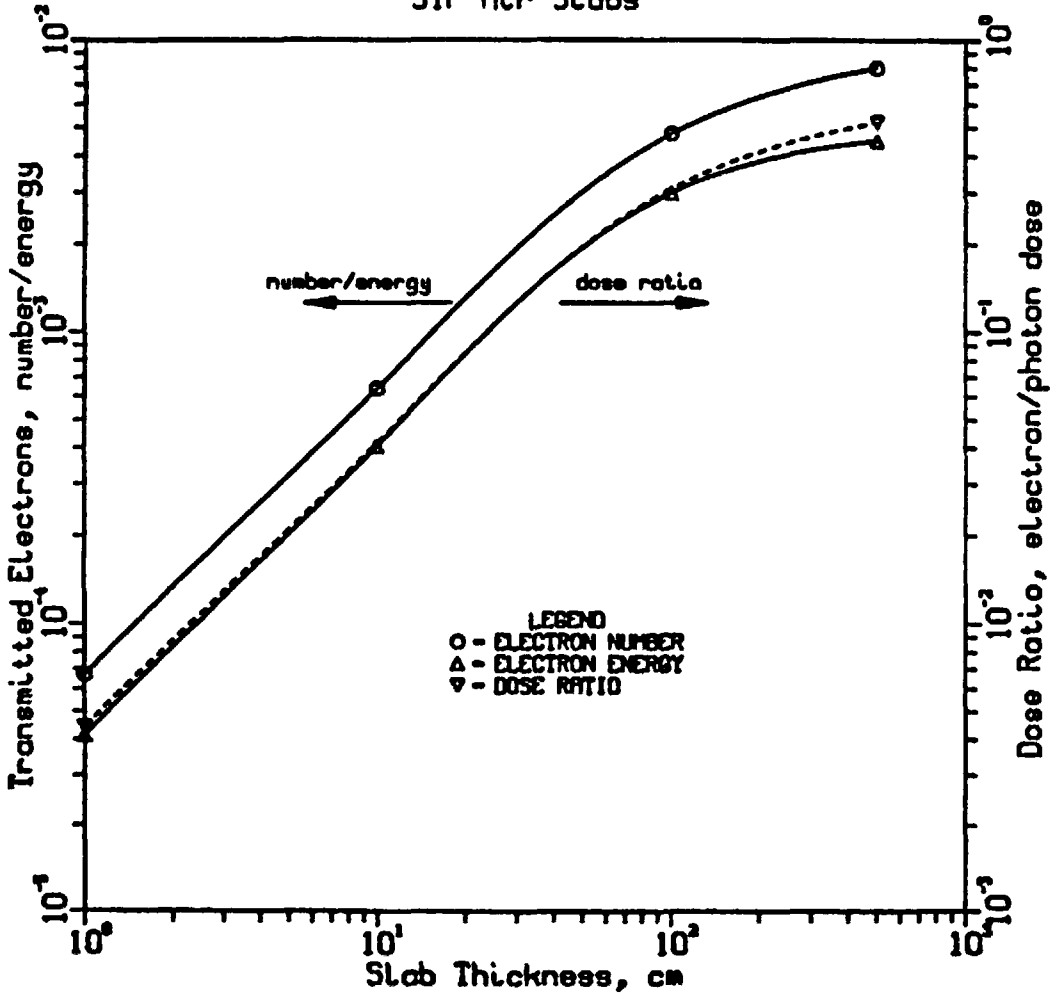


Figure 3. Transmission of Recoil Electron Particle Number, Energy, and Absorbed Dose Ratio in Air.

Electron Deposition in EPR
(Normalized to one incident particle)
versus Depth Into Slab
EPR Slab Thickness = .1524 cm (60 mil)

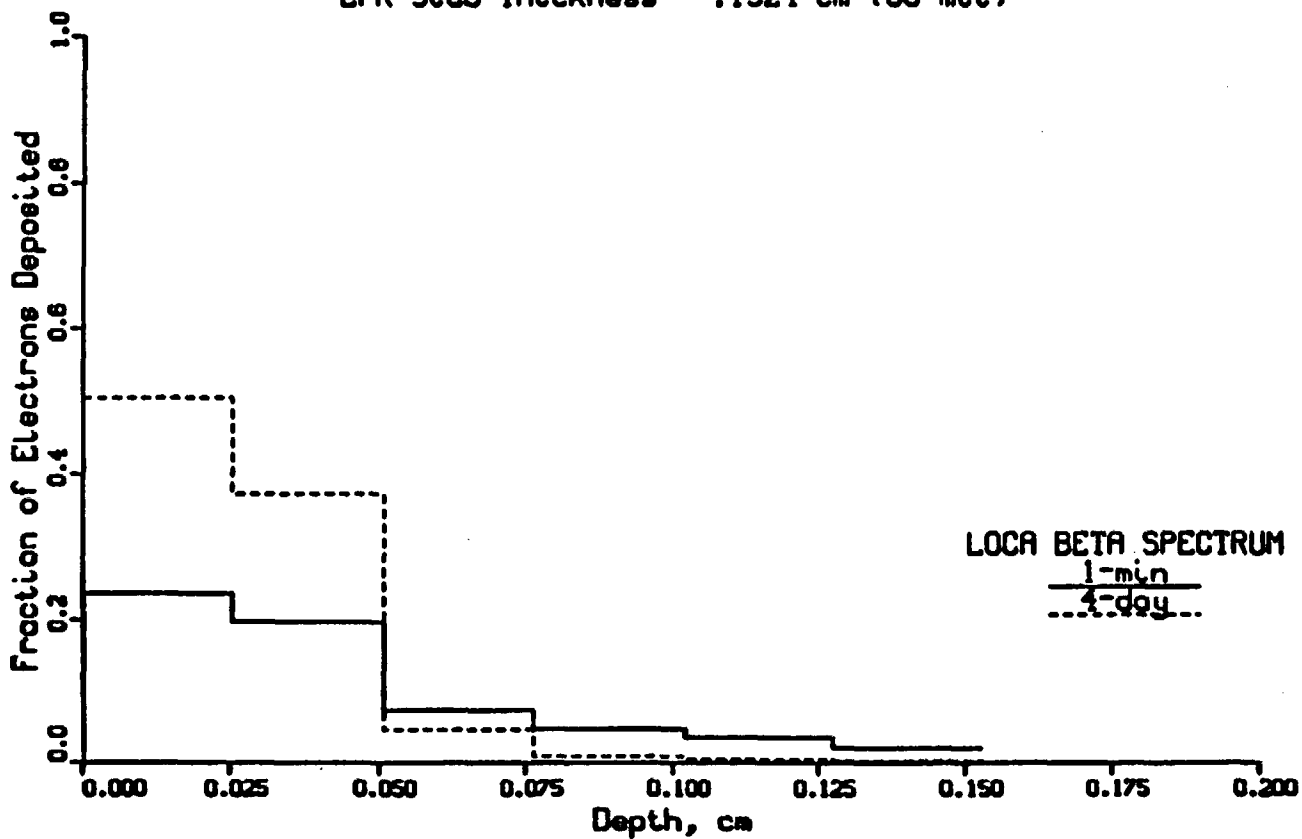


Figure 4. Electron Charge Deposition in EPR from LOCA Source
Electron Exposure.

Electron Deposition in EPR
 (Normalized to one incident particle)
 versus Depth Into Slab
 EPR Slab Thickness = .1524 cm (60 mil)

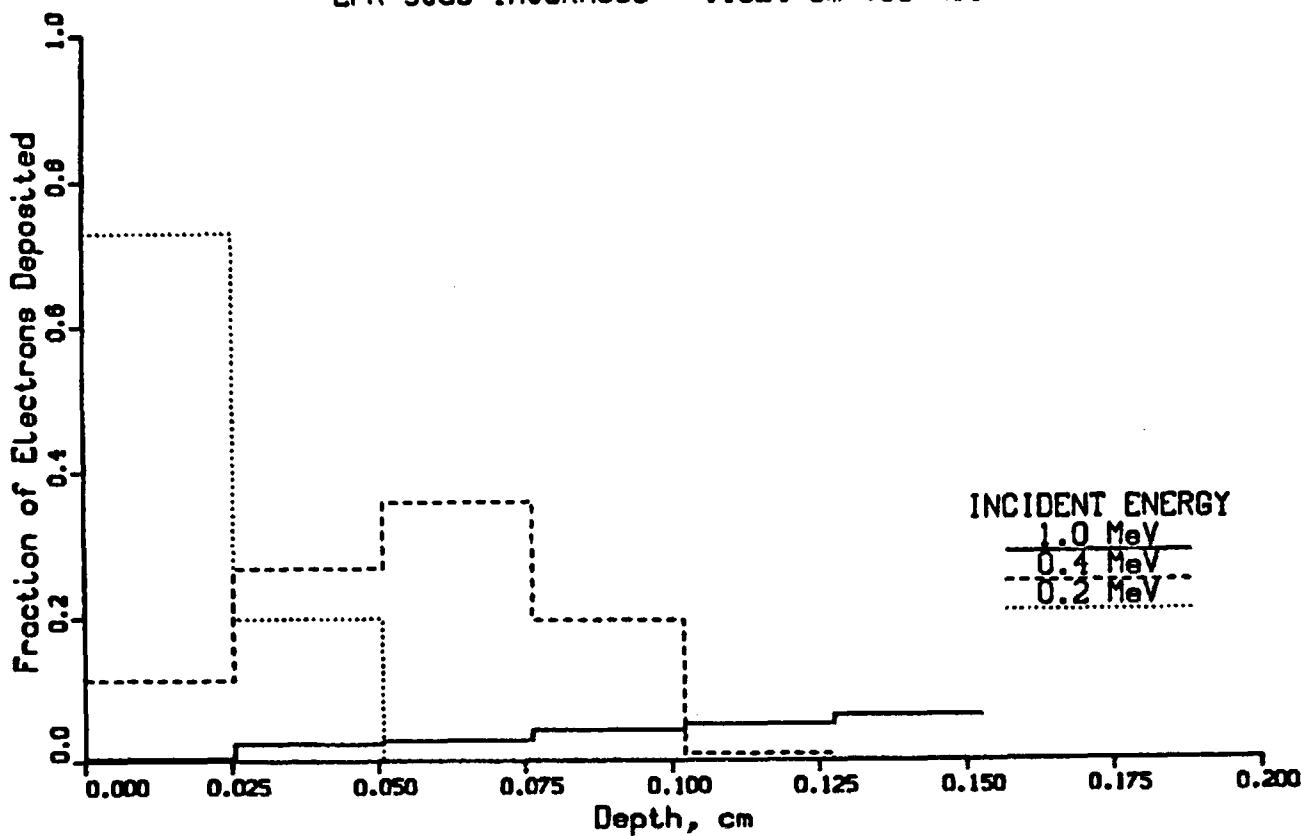


Figure 5. Electron Charge Deposition in EPR from Monoenergetic Electron Exposure.

Maximum Beam Deflection versus
Raster Coil Current
beam energy = 1.0 MeV
target-coil separation = 70 cm

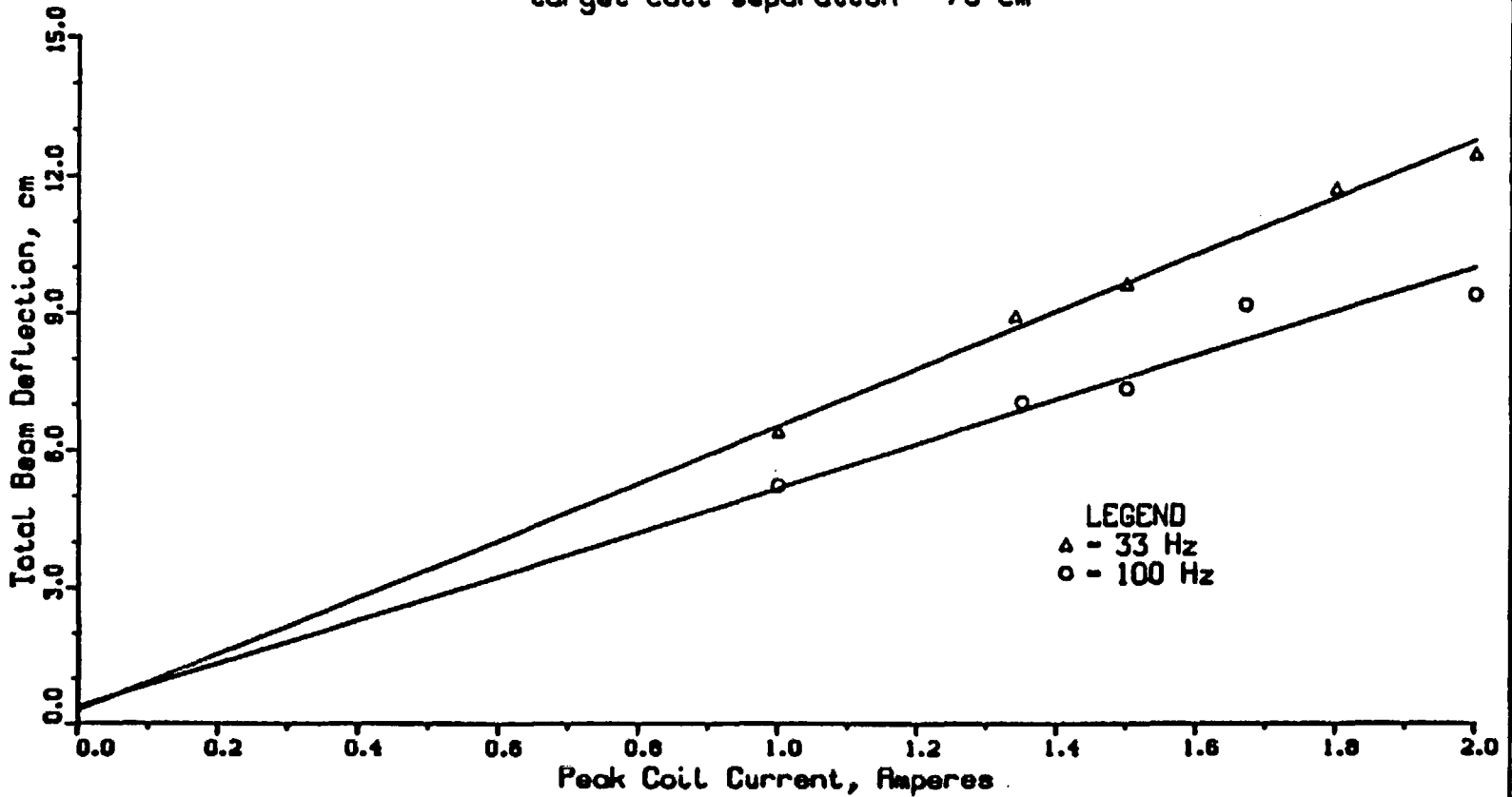


Figure 6. Maximum Electron Beam Deflection as a Function of Raster Coil Current.

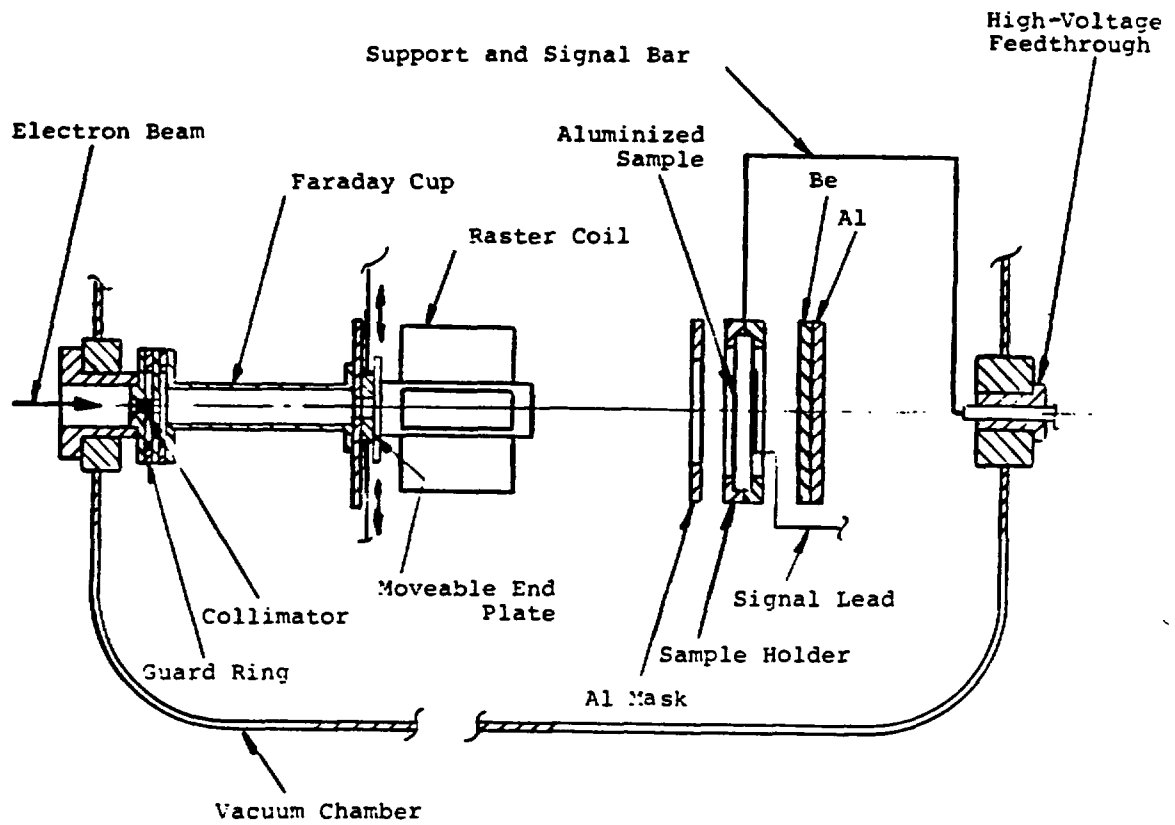


Figure 7a. Schematic of Experiment Orientation In Vacuum Chamber.

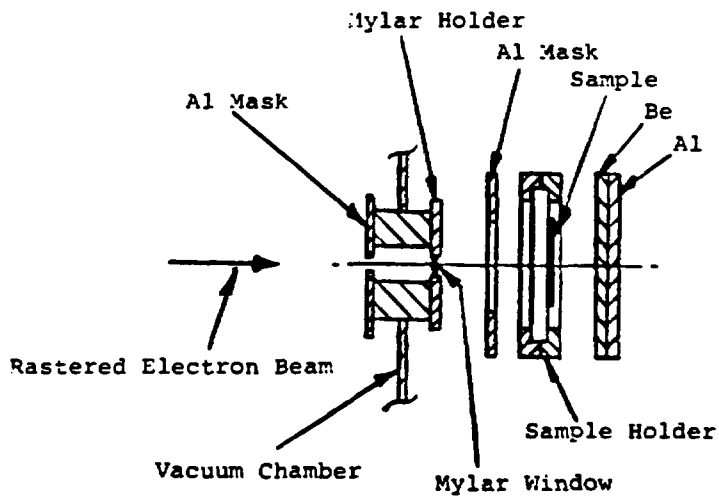


Figure 7b. Schematic of Experiment Orientation Outside of Vacuum Chamber.

Figure 8. Schematic of Material Sample Holder Configuration.

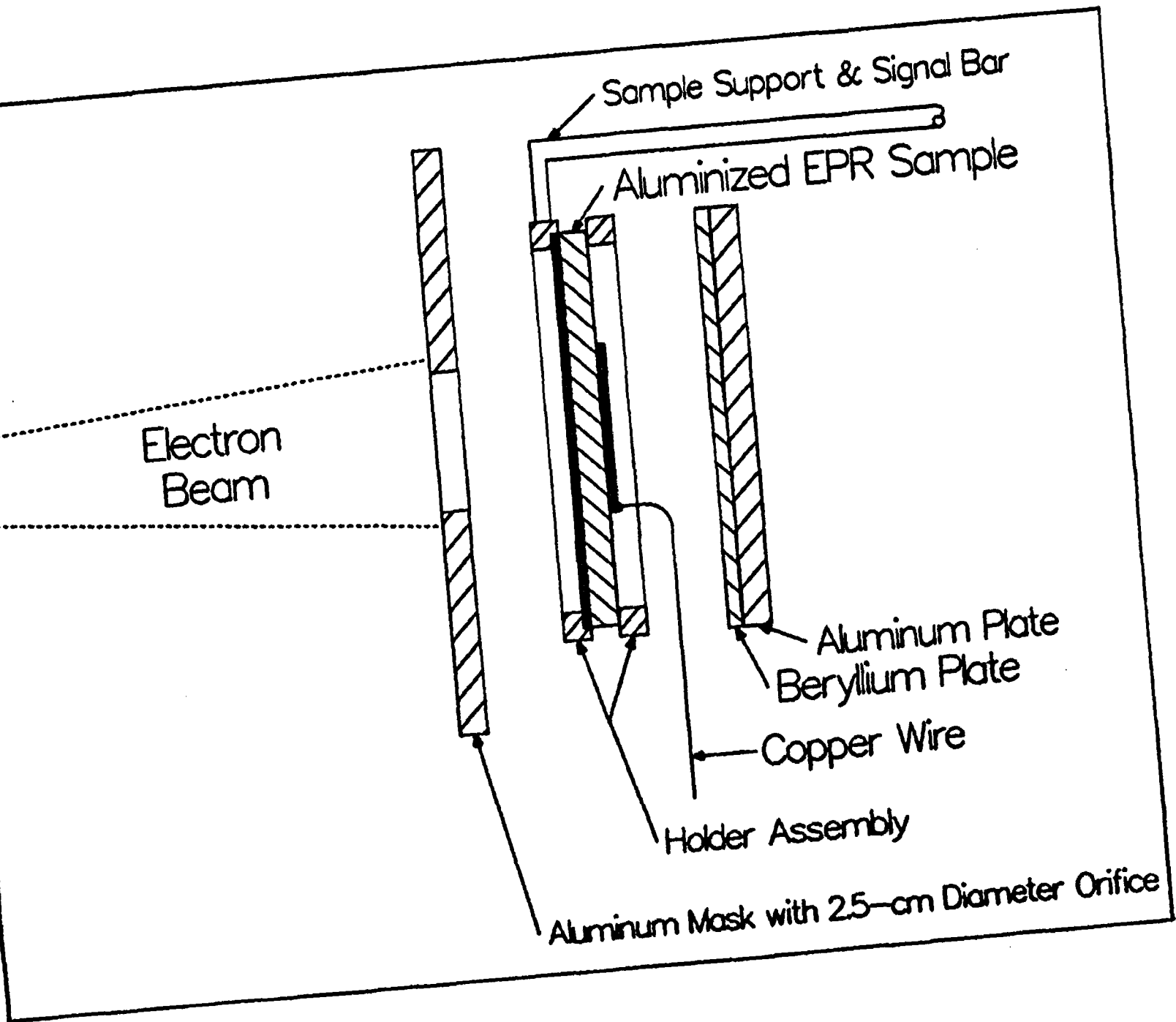
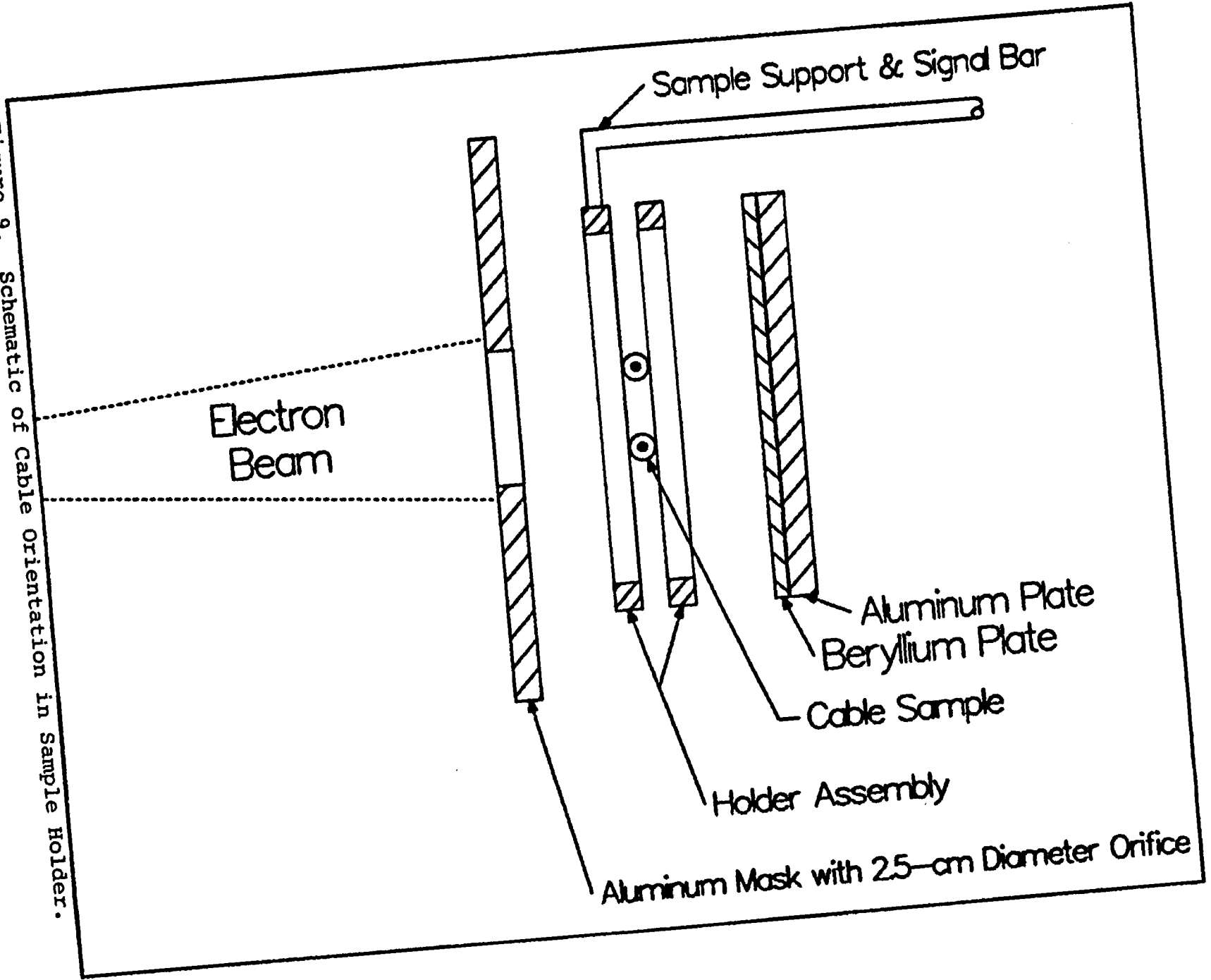


Figure 9. Schematic of Cable Orientation in Sample Holder.



Beryllium Stopper Current versus Faraday Cup Current

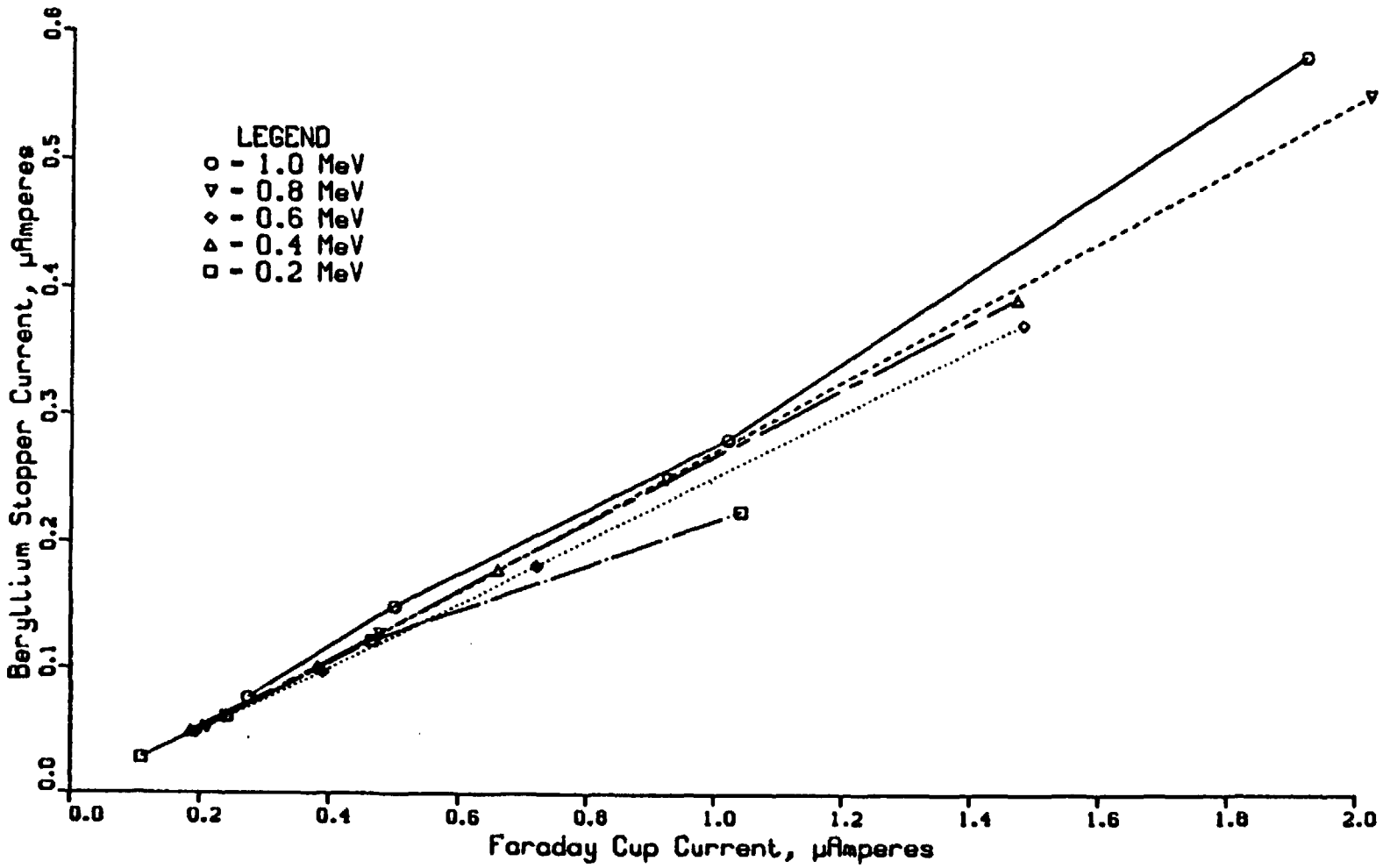


Figure 10. Beryllium Stopper Current Versus Faraday Cup Current.

Dose Rate versus
Beryllium Stopper Current
(Lines are calculated values)

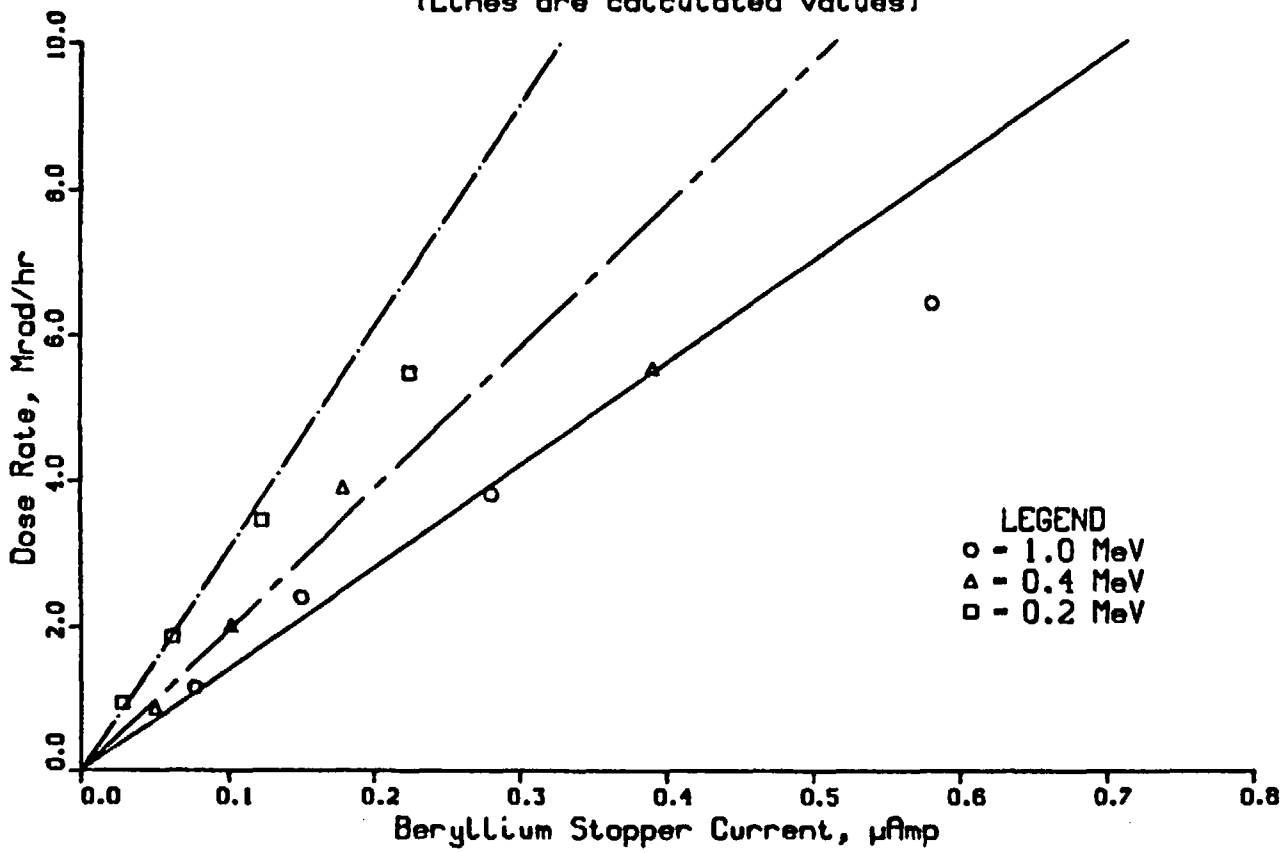


Figure 11. Measured and Calculated Dose Rates Versus Beryllium Stopper Currents.

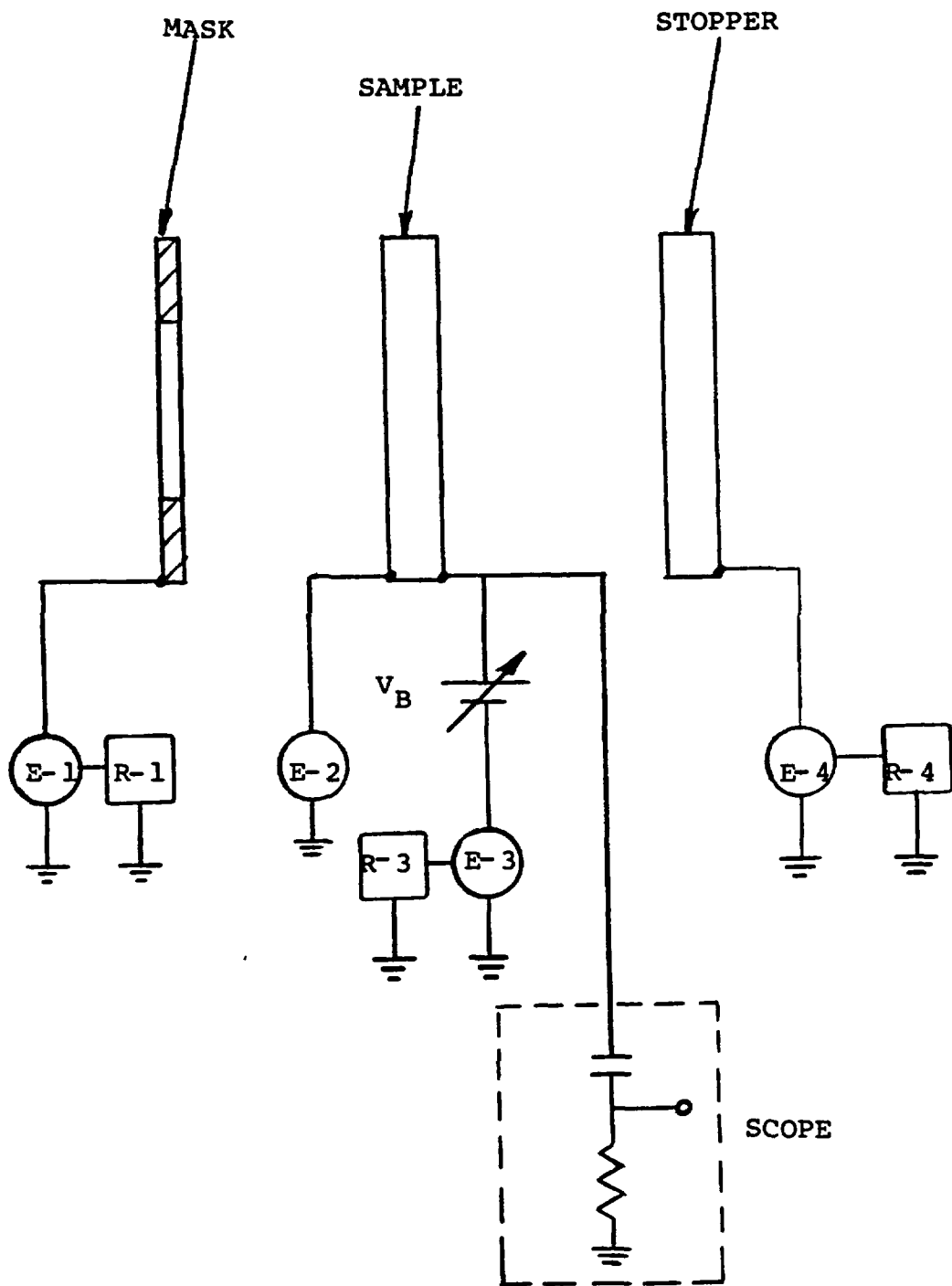


Figure 12. Schematic of Signal Measuring Configuration

Front and Back Surface Currents
(Normalized to Faraday Cup Current)
versus Back Surface Bias Voltage
beam energy = 1.0 MeV

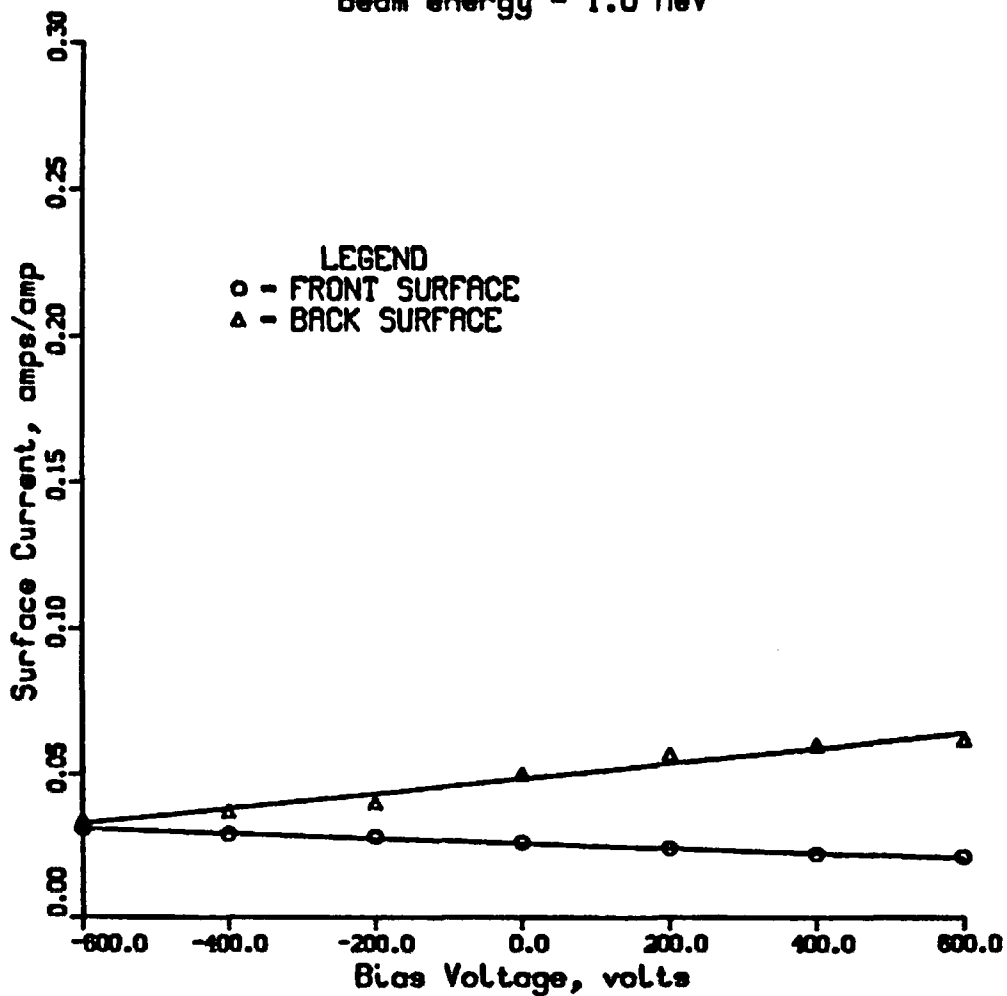


Figure 13. Measured Surface Currents Versus Bias Voltage for 1.0 MeV Source Electrons.

Front and Back Surface Currents
 (Normalized to Faraday Cup Current)
 versus Back Surface Bias Voltage
 beam energy = 0.6 MeV

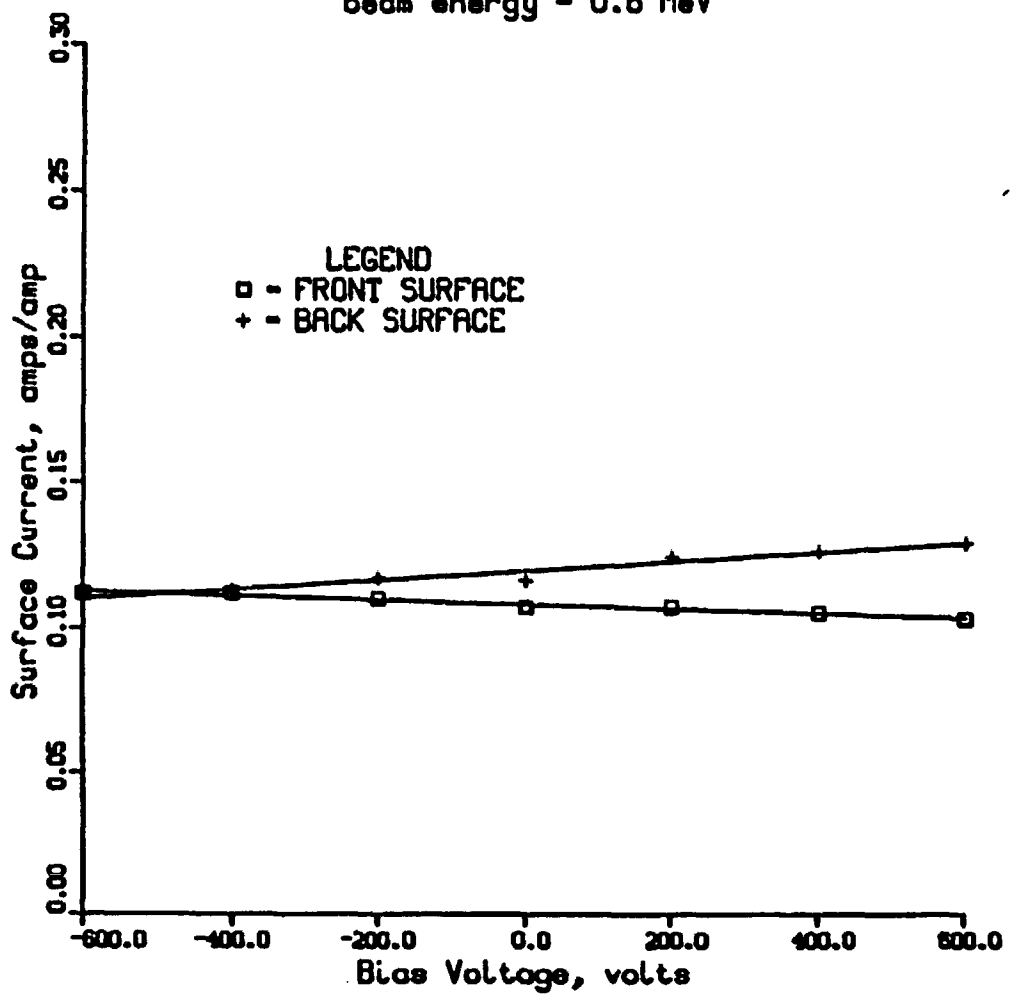


Figure 14. Measured Surface Currents Versus Bias Voltage for 0.6 MeV Source Electrons.

Front and Back Surface Currents
(Normalized to Faraday Cup Current)
versus Back Surface Bias Voltage
beam energy = 0.4 MeV

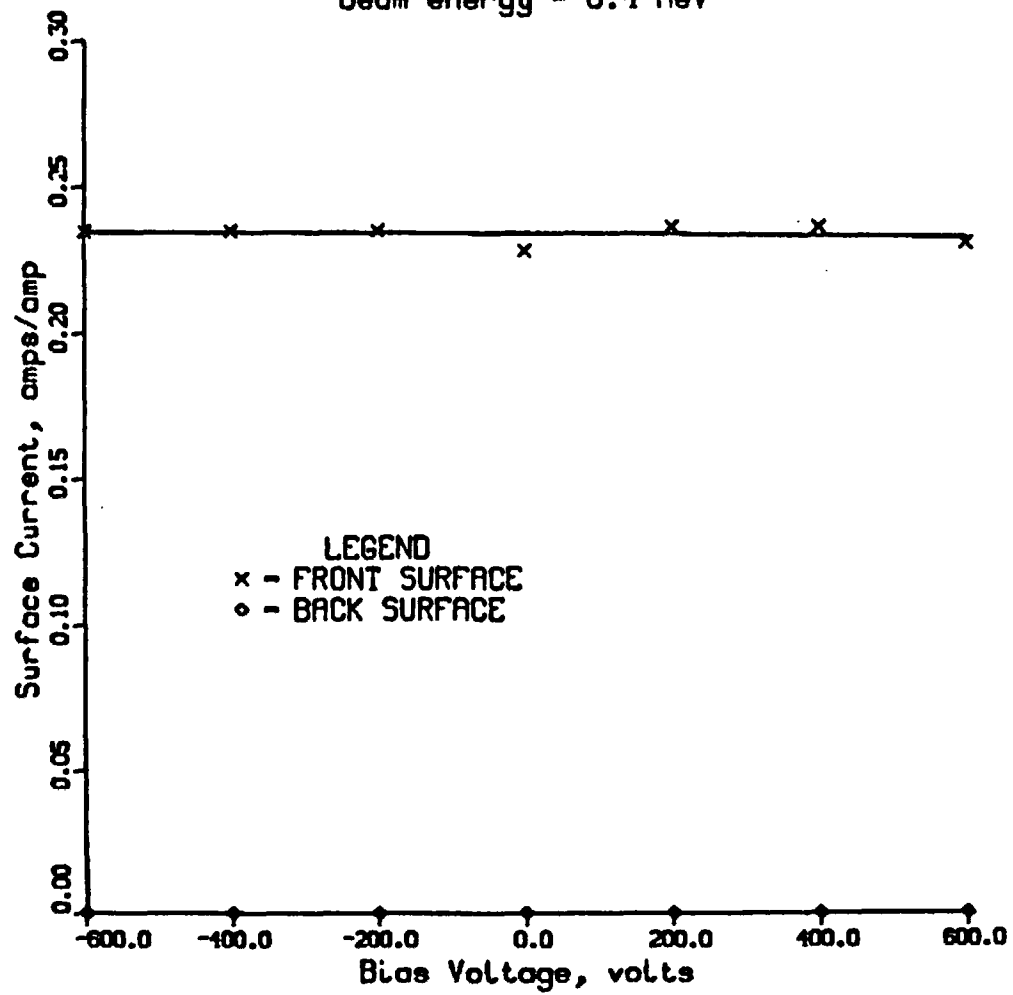


Figure 15. Measured Surface Currents Versus Back Surface Bias Voltage for 0.4 MeV Source Electrons.

Front and Back Surface Currents
(Normalized to Faraday Cup Current)
versus Front Surface Bias Voltage
beam energy = 0.4 MeV

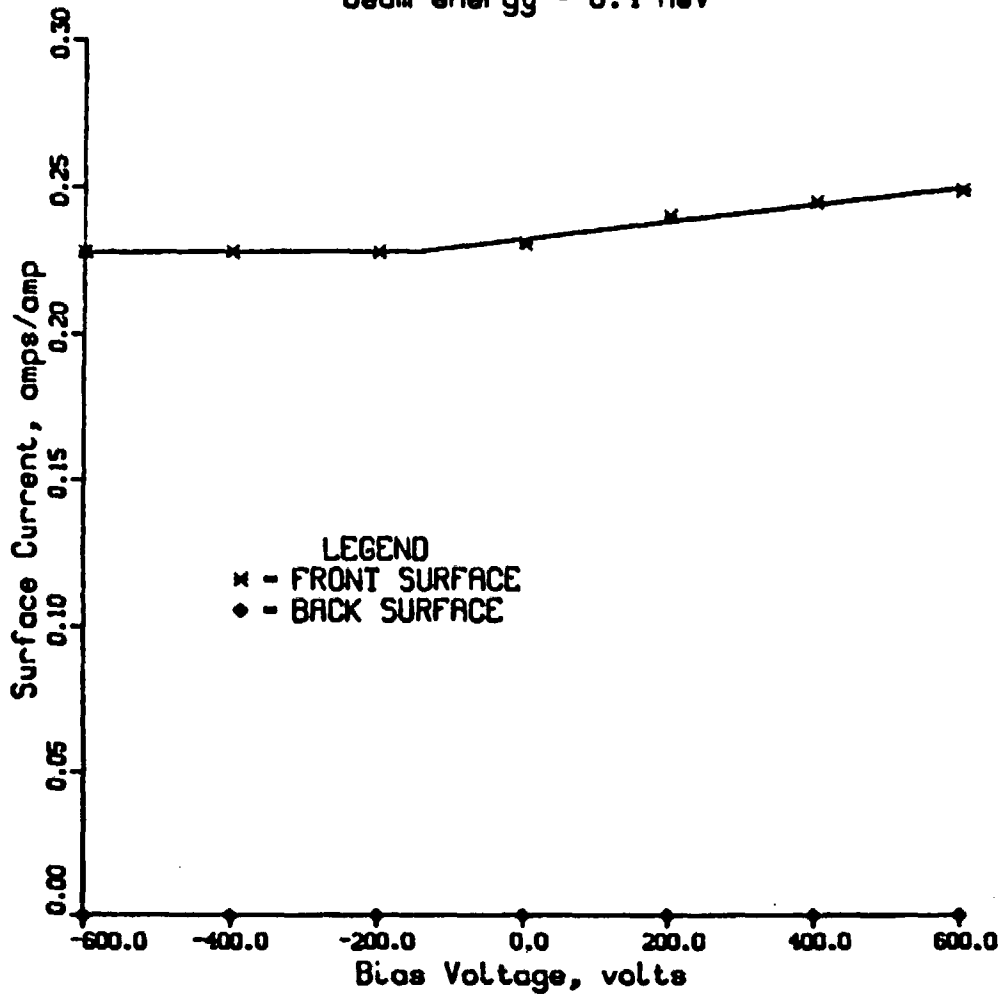


Figure 16. Measured Surface Currents Versus Front Surface Bias Voltage for 0.4 MeV Source Electrons.

Front Surface Current
(Normalized to Faraday Cup Current)
versus Front Surface Bias Voltage
beam energy = 0.4 MeV

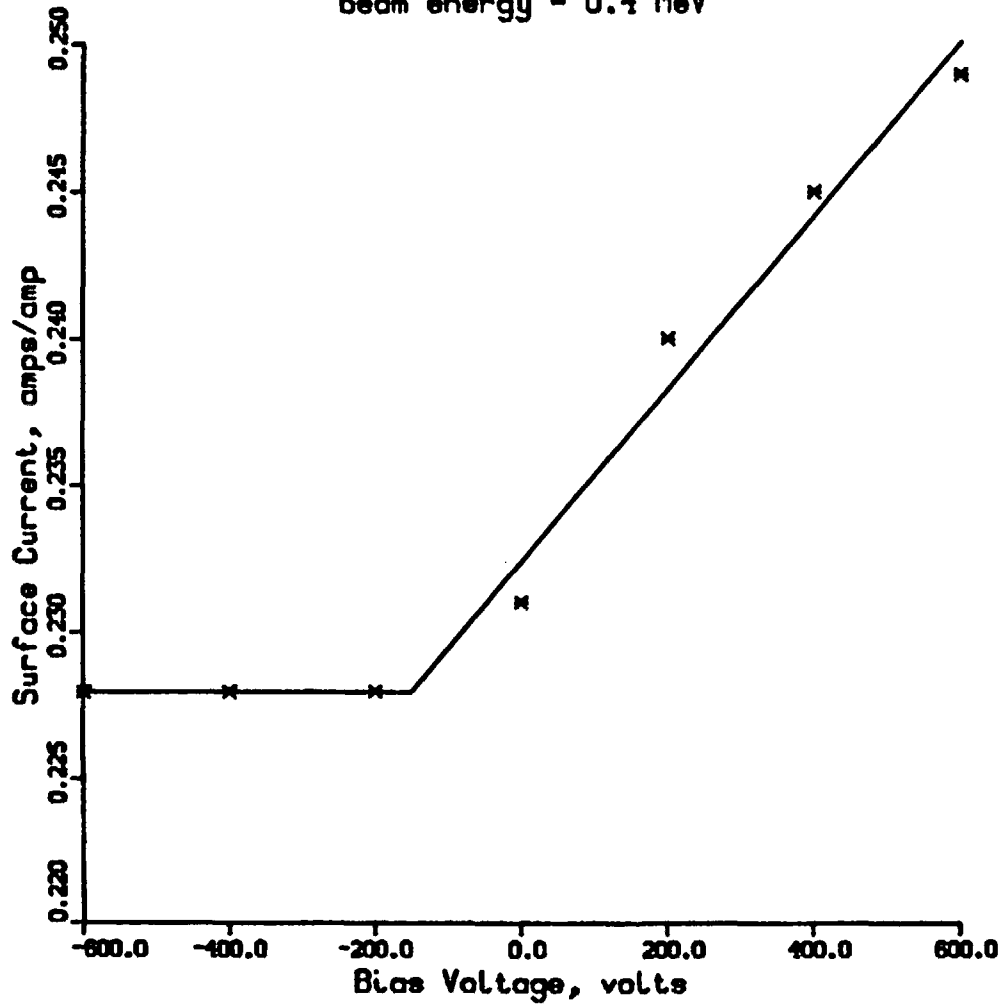


Figure 17. Measured Front Surface Current Versus Front Surface Bias Voltage (Expanded Scale) for 0.4 MeV Source Electrons.

Front and Back Surface Currents
(Normalized to Faraday Cup Current)
versus Back Surface Bias Voltage
beam energy = 0.2 MeV

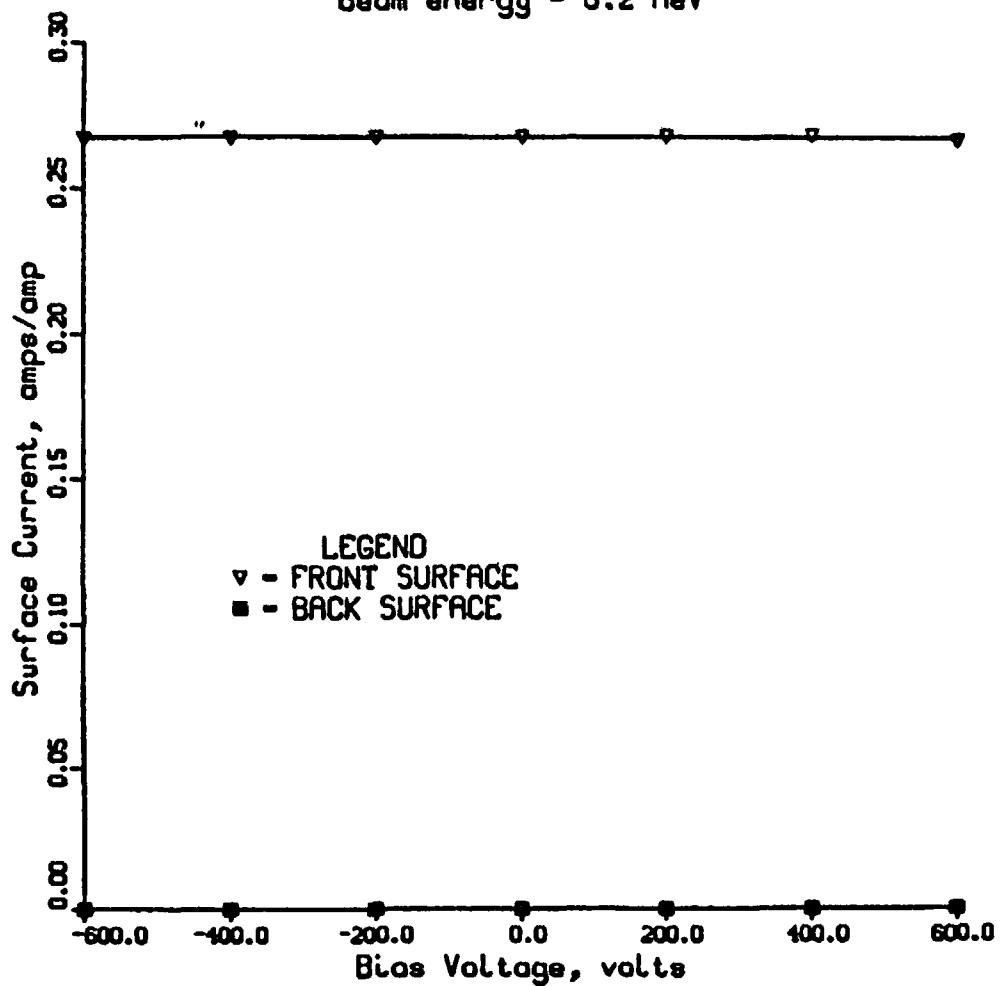


Figure 18. Measured Surface Currents Versus Bias Voltage for 0.2 MeV Source Electrons.

Front Surface Equilibrium Voltage
as a function of
Beam Energy

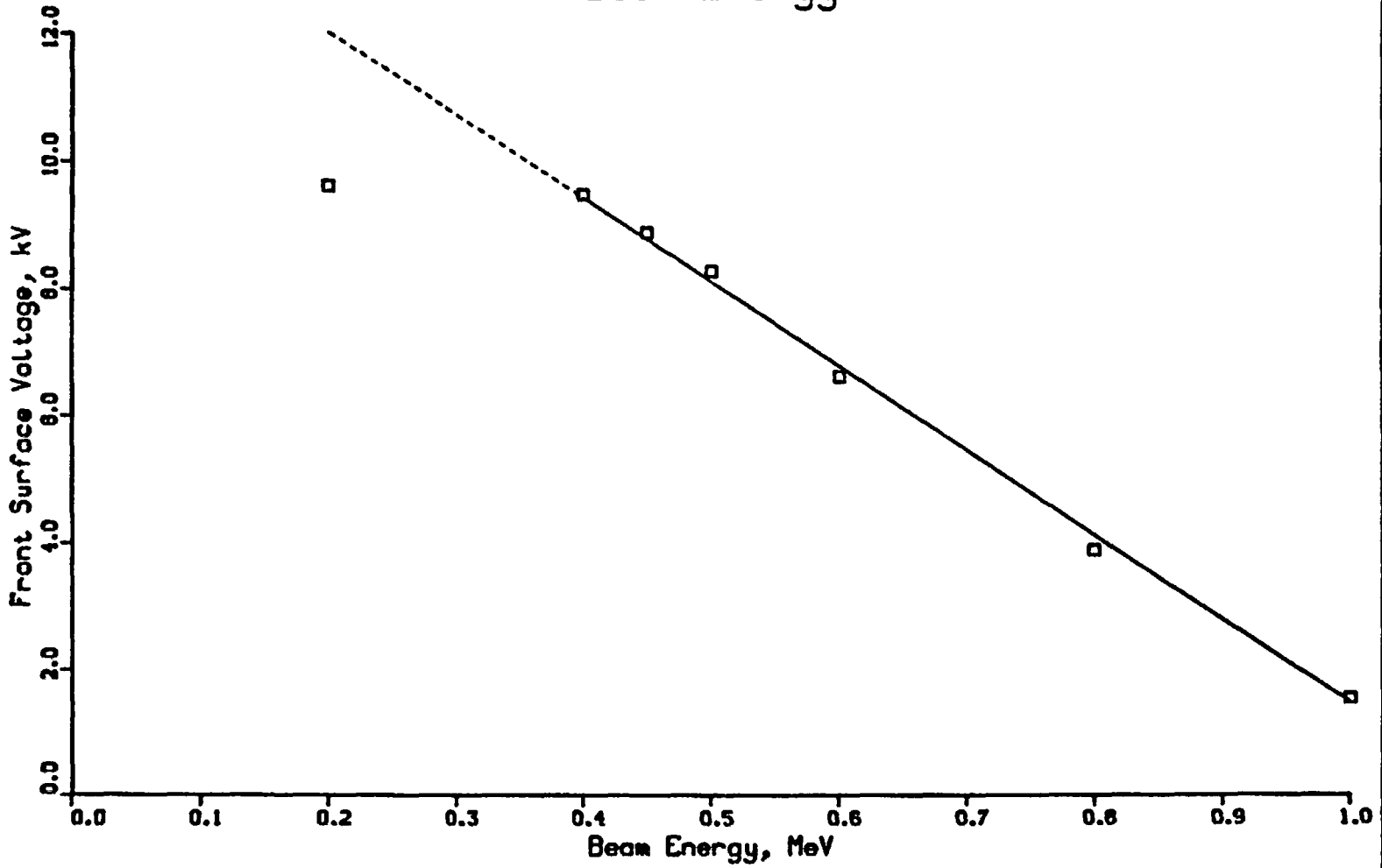


Figure 19. Front Surface Equilibrium Voltage as a Function of Source Beam Energy.

Back Surface Current
as a function of
Beam Energy

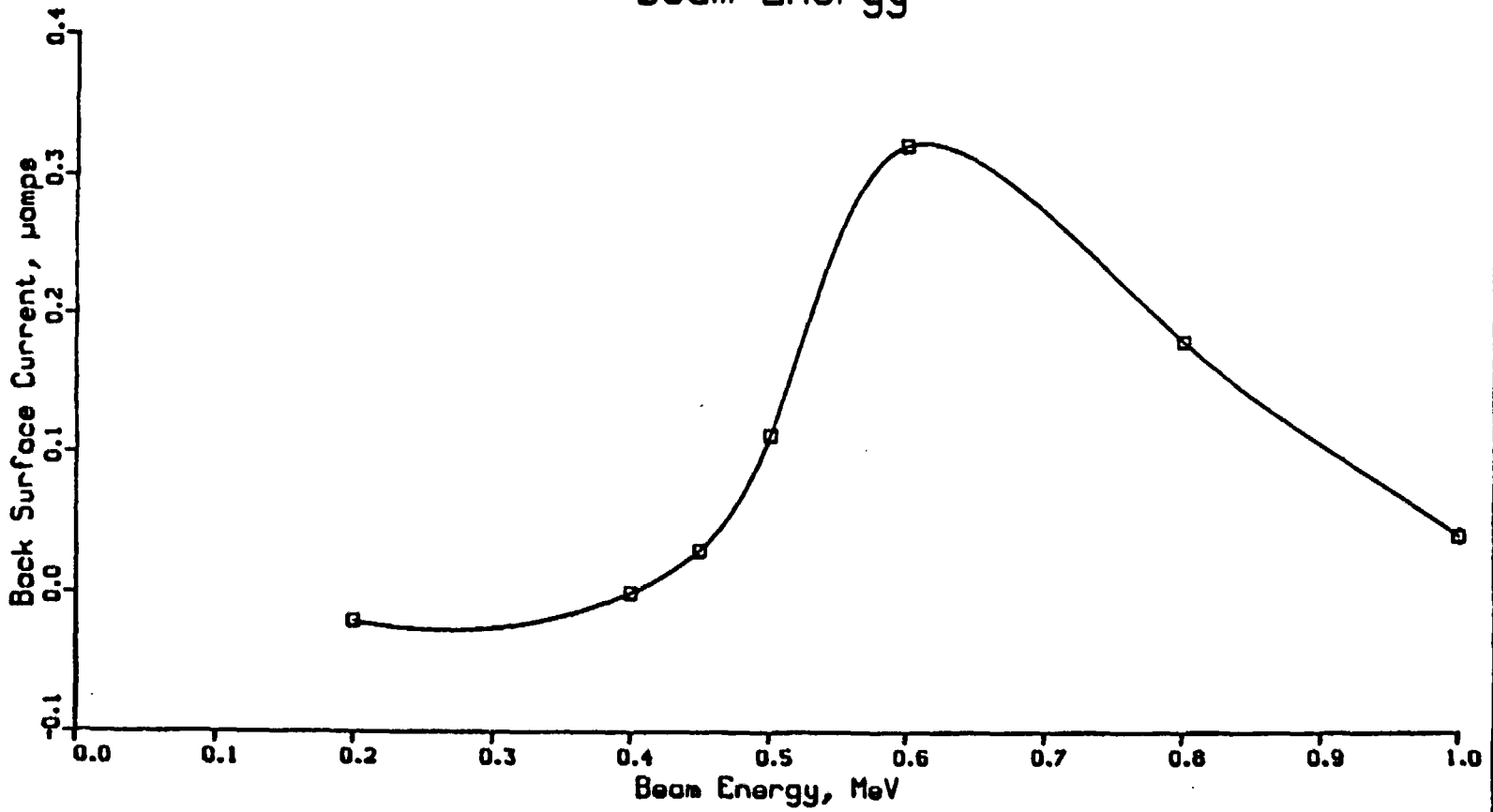


Figure 20. Back Surface Current as a Function of Source Beam Energy.

EPR Front Surface Voltage versus
Time, Before and After Irradiation
With 1.0 MeV Electrons
beam energy = 0.2 MeV

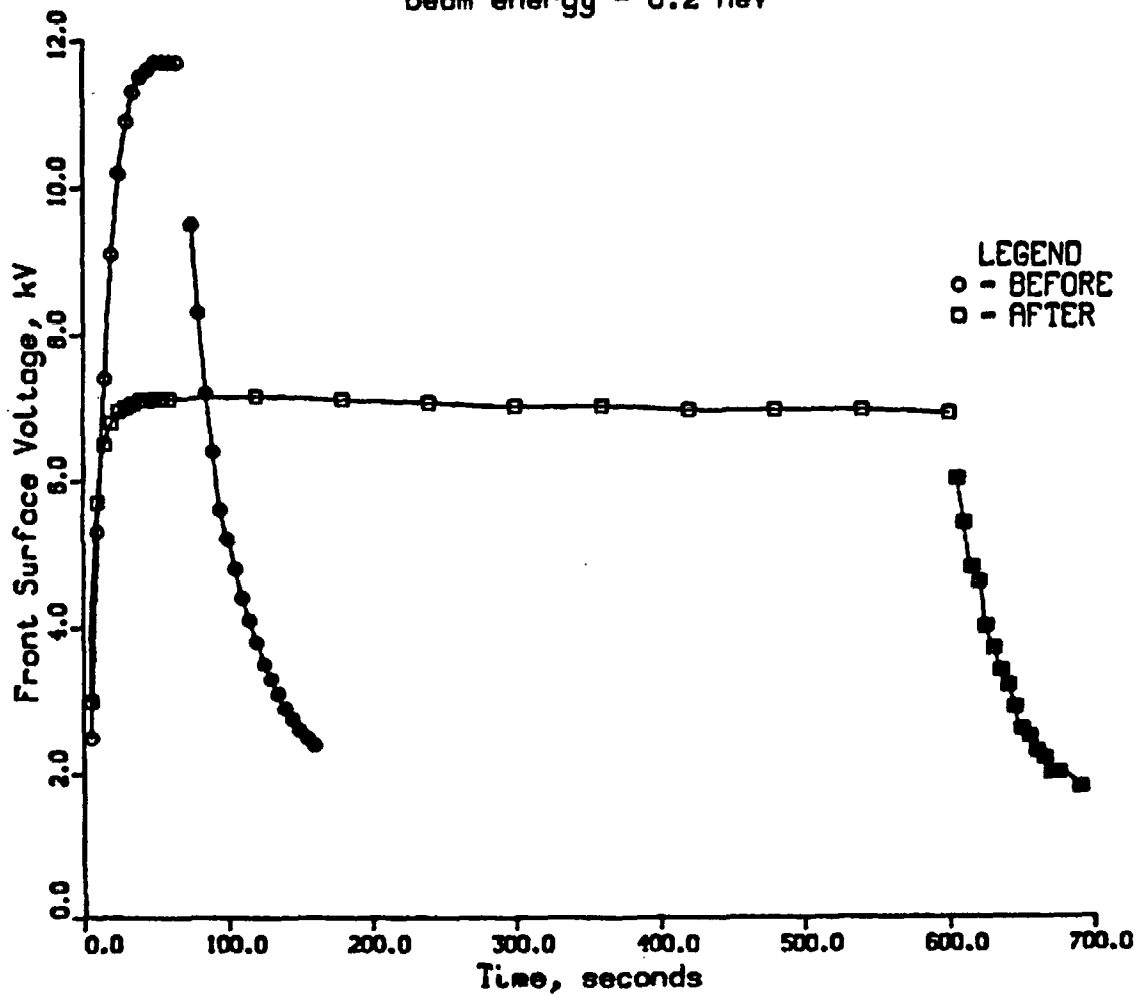


Figure 21. EPR Front Surface Voltage Versus Time for 0.2 MeV Source Electrons.

EPR Front Surface Voltage versus
Time, Before and After Irradiation
With 1.0 MeV Electrons
beam energy = 0.45 MeV

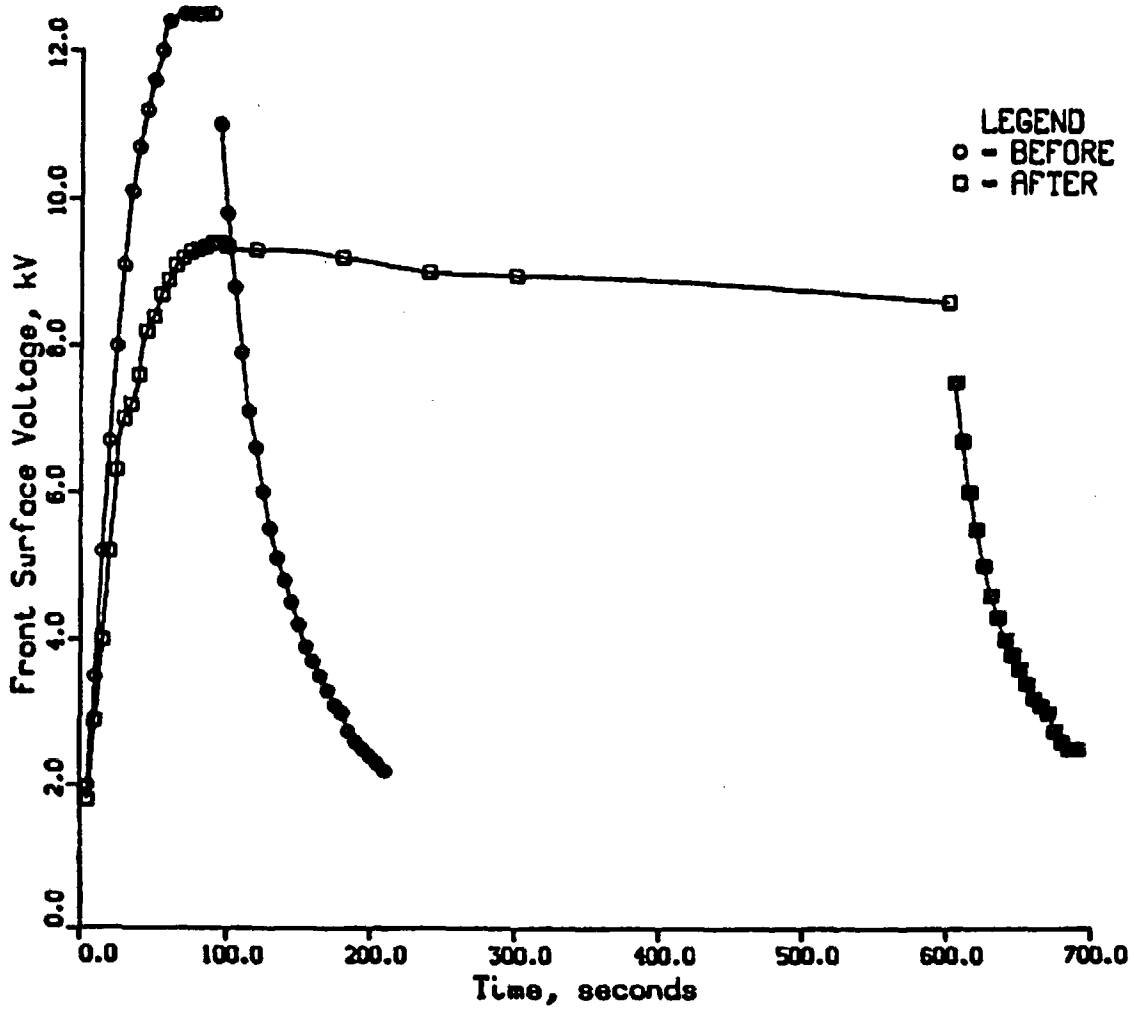


Figure 22. EPR Front Surface Voltage Versus Time for 0.45 MeV Source Electrons.

Front and Back Surface Currents
(Normalized to Faraday Cup Current)
versus Back Surface Bias Voltage
beam energy = 1.0 MeV, irradiation in air

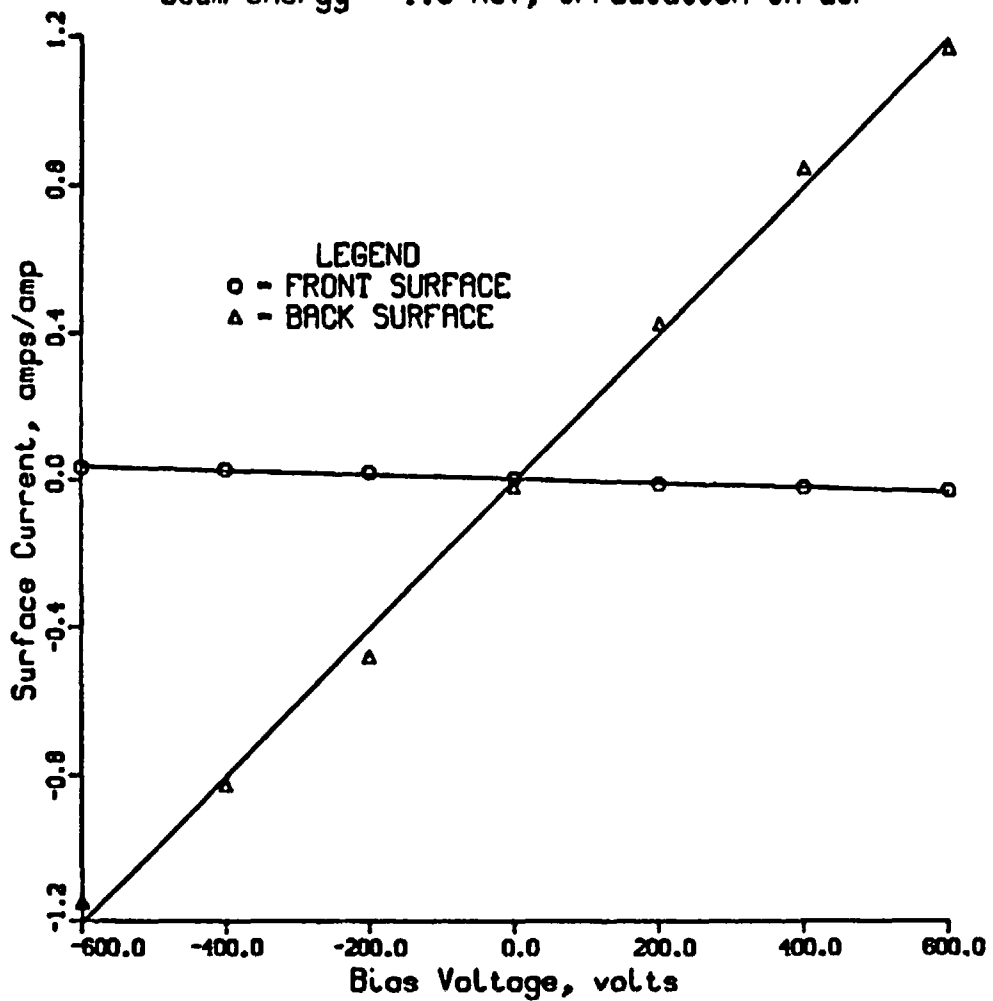


Figure 23. Measured Surface Currents Versus Bias Voltage for 1.0 MeV Source Electrons in Air.

Front and Back Surface Currents
 (Normalized to Faraday Cup Current)
 versus Back Surface Bias Voltage
 beam energy = 0.4 MeV, irradiation in air

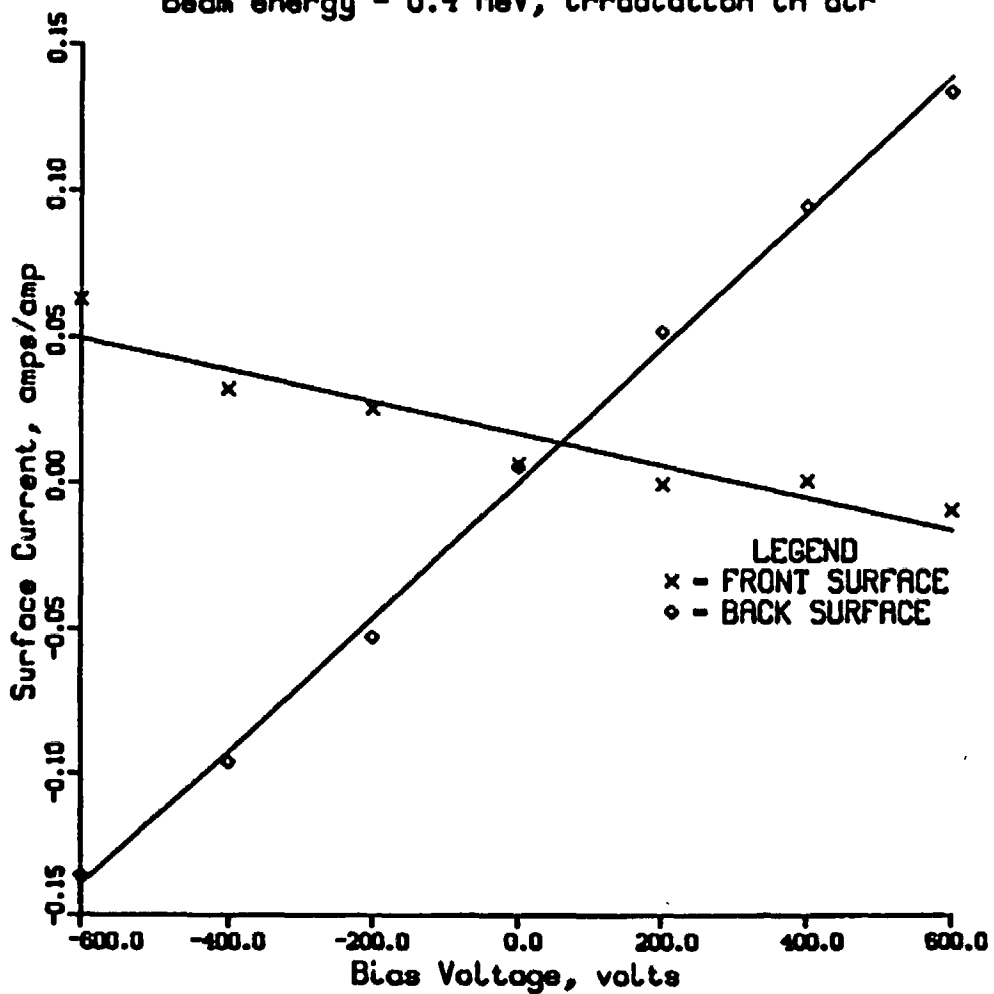


Figure 24. Measured Surface Currents Versus Bias Voltage for 0.4 MeV Source Electrons in Air.

TABLE 1. Incident Beam Current Partition for 1.0 MeV Source
Electrons in Vacuum Environment*

<u>VB</u>	<u>IM</u>	<u>IFS</u>	<u>IBS</u>	<u>IBE</u>	<u>ISUM</u>	<u>IFC</u>	<u>RATIO</u>
600	2.122	0.060	0.177	0.500	2.859	2.850	1.003
400	2.048	0.061	0.170	0.510	2.789	2.825	0.987
200	2.042	0.069	0.160	0.523	2.794	2.830	0.987
0	2.042	0.073	0.142	0.542	2.799	2.835	0.987
-200	2.042	0.079	0.114	0.560	2.795	2.840	0.984
-400	2.029	0.083	0.106	0.570	2.788	2.835	0.983
-600	2.037	0.089	0.096	0.576	2.798	2.830	0.989

*All currents in units of microamps

VB = Bias voltage on back surface (volts)
IM = Mask current
IFS = Front surface current
IBS = Back surface current
IBE = Beryllium stopper current
ISUM = Sum of IM, IFS, IBS, and IBE
IFC = Faraday Cup current
RATIO = ISUM/IFC

TABLE 2. Incident Beam Current Partition for 0.2 MeV Source
Electrons in Vacuum Environment*

<u>VB</u>	<u>IM</u>	<u>IFS</u>	<u>IBS</u>	<u>IBE</u>	<u>ISUM</u>	<u>IFC</u>	<u>RATIO</u>
600	1.130	0.400	0.000	0.000	1.530	1.510	1.013
400	1.130	0.400	0.000	0.000	1.530	1.500	1.020
200	1.130	0.400	0.000	0.000	1.530	1.500	1.020
0	1.130	0.400	0.000	0.000	1.530	1.500	1.020
-200	1.130	0.400	0.000	0.000	1.530	1.500	1.020
-400	1.130	0.400	0.000	0.000	1.530	1.500	1.020
-600	1.130	0.400	0.000	0.000	1.530	1.500	1.020

*All currents in units of microamps

VB = Bias voltage on back surface (volts)
 IM = Mask current
 IFS = Front surface current
 IBS = Back surface current
 IBE = Beryllium stopper current
 ISUM = Sum of IM, IFS, IBS, and IBE
 IFC = Faraday Cup current
 RATIO = ISUM/IFC

TABLE 3. Comparison of Measured And Calculated Fraction of Incident Electrons Stopped Within EPR Volume*

<u>EB</u>	<u>#e(calc)</u>	<u>#e(meas)</u>	<u>RATIO</u>
0.2	0.998	1.000	0.998
0.4	1.004	1.000	1.004
0.6	0.904	0.937	0.965
1.0	0.222	0.284	0.782

*Fraction of incident electrons normalized to one incident particle

EB = Electron beam energy (MeV)
 #e(calc) = Fraction of incident electrons in EPR calculated by TIGER code
 #e(meas) = Fraction of incident electrons in EPR measured during experiment
 RATIO = #e(calc)/#e(meas)

TABLE 4. Incident Beam Current Partition for 1.0 MeV Source
Electrons in Ambient Air Environment*

<u>VB</u>	<u>IM1</u>	<u>IM2</u>	<u>IFS</u>	<u>IBS</u>	<u>IBE</u>	<u>ISUM</u>	<u>IFC</u>	<u>RATIO</u>
600	3.167	0.040	-0.115	4.700	-4.000	3.792	4.020	0.943
400	3.167	0.060	-0.093	3.400	-2.900	3.634	4.020	0.904
200	3.167	0.090	-0.062	1.700	-1.200	3.695	4.020	0.919
0	3.200	0.110	0.008	-0.080	0.130	3.368	4.020	0.838
-200	3.167	0.013	0.069	-1.930	1.950	3.269	4.020	0.813
-400	3.167	0.150	0.103	-3.300	3.200	3.320	4.000	0.830
-600	3.167	0.160	0.128	-4.600	4.300	3.155	4.000	0.789

*All currents in units of microamps

VB = Bias voltage on back surface (volts)
IM1 = In-vacuum mask current
IM2 = In-air mask current
IFS = Front surface current
IBS = Back surface current
IBE = Beryllium stopper current
ISUM = Sum of IM1, IM2, IFS, IBS, and IBE
IFC = Faraday Cup current
RATIO = ISUM/IFC

TABLE 5. Incident Beam Current Partition for 0.4 MeV Source
Electrons in Ambient Air Environment*

<u>VB</u>	<u>IM1</u>	<u>IM2</u>	<u>IFS</u>	<u>IBS</u>	<u>IBE</u>	<u>ISUM</u>	<u>IFC</u>	<u>RATIO</u>
600	3.072	0.190	-0.039	0.520	-0.085	3.658	3.920	0.933
400	3.105	0.170	0.000	0.370	-0.066	3.579	3.950	0.906
200	3.116	0.250	-0.005	0.200	-0.045	3.516	3.950	0.890
0	3.183	0.300	0.025	0.020	0.001	3.530	4.080	0.865
-200	3.161	0.300	0.100	-0.215	0.047	3.393	4.020	0.844
-400	3.128	0.320	0.127	-0.385	0.070	3.260	4.000	0.815
-600	3.128	0.240	0.250	-0.540	0.087	3.165	3.980	0.795

*All currents in units of microamps

VB = Bias voltage on back surface (volts)
IM1 = In-vacuum mask current
IM2 = In-air mask current
IFS = Front surface current
IBS = Back surface current
IBE = Beryllium stopper current
ISUM = Sum of IM1, IM2, IFS, IBS, and IBE
IFC = Faraday Cup current
RATIO = ISUM/IFC

DISTRIBUTION:

U.S. NRC Distribution Contractor
7300 Pearl Street
Bethesda, MD 20014
375 copies for RV

Ansaldo Impianti
Centro Sperimentale del Boschetto
Corso F.M. Perrone, 118
16161 Genova
ITALY
Attn: C. Bozzolo

Ansaldo Impianti
Via Gabriele D'Annunzio, 113
16121 Genova
ITALY
Attn: S. Grifoni

ASEA-ATOM
Department KRD
Box 53
S-721 04
Vasteras
SWEDEN
Attn: A. Kjellberg

ASEA-ATOM
Department TQD
Box 53
S-721 04
Vasteras
SWEDEN
Attn: T. Granberg

ASEA KABEL AB
P.O. Box 42 108
S-126 12
Stockholm
SWEDEN
Attn: B. Dellby

Atomic Energy of Canada, Ltd.
Chalk River Nuclear Laboratories
Chalk River, Ontario K0J 1J0
CANADA
Attn: G. F. Lynch

Atomic Energy of Canada, Ltd.
1600 Dorchester Boulevard West
Montreal, Quebec H3H 1P9
CANADA
Attn: S. Nish

Bhabha Atomic Research Centre
Health Physics Division
BARC
Bombay-85
INDIA
Attn: S. K. Mehta

British Nuclear Fuels Ltd.
Springfields Works
Salwick, Preston
Lancs
ENGLAND
Attn: W. G. Cunliff, Bldg 334

Brown Boveri Reaktor GMBH
Postfach 5143
D-6800 Mannheim 1
WEST GERMANY
Attn: R. Schemmel

Bundesanstalt fur Materialprufung
Unter den Eichen 87
D-1000 Berlin 45
WEST GERMANY
Attn: K. Wundrich

CEA/CEN-FAR
Departement de Surete Nucleaire
Service d'Analyse Fonctionnelle
B.P. 6
92260 Fontenay-aux-Roses
FRANCE
Attn: M. Le Meur
J. Henry

CERN
Laboratoire 1
CH-1211 Geneve 23
SWITZERLAND
Attn: H. Schonbacher

Canada Wire and Cable Limited
Power & Control Products Division
22 Commercial Road
Toronto, Ontario
CANADA M4G 1Z4
Attn: Z. S. Paniri

Commissariat a l'Energie Atomique
ORIS/LABRA
BP N° 21
91190 Gif-Sur-Yvette
FRANCE
Attn: G. Gaussens
J. Chenion
F. Carlin

Commissariat a l'Energie Atomique
CEN Cadarche DRE/STRE
BP N° 1
13115 Saint Paul Lez Durance
FRANCE
Attn: J. Campan

Conductores Monterrey, S. A.
P.O. Box 2039
Monterrey, N. L.
MEXICO
Attn: P. G. Murga

Electricite de France
Direction des Etudes et Recherches
1, Avenue du General de Gaulle
92141 CLAMART CEDEX
FRANCE
Attn: J. Roubault
L. Deschamps

Electricite de France
Direction des Etudes et Recherches
Les Renardieres
Boite Postale n° 1
77250 MORET SUR LORING
FRANCE
Attn: Ph. Roussarie
V. Deglon
J. Ribot

EURATOM
Commission of European Communities
C.E.C. J.R.C.
21020 Ispra (Varese)
ITALY
Attn: G. Mancini

FRAMATOME
Tour Fiat - Cedex 16
92084 Paris La Defense
FRANCE
Attn: G. Chauvin
E. Raimondo

Furukawa Electric Co., Ltd.
Hiratsuka Wire Works
1-9 Higashi Yawata - 5 Chome
Hiratsuka, Kanagawa Pref
JAPAN 254
Attn: E. Oda

Gesellschaft fur Reaktorsicherheit
(GRS) mbH
Glockengasse 2
D-5000 Koln 1
WEST GERMANY
Attn: Library

Health & Safety Executive
Thames House North
Milbank
London SW1P 4QJ
ENGLAND
Attn: W. W. Ascroft-Hutton

ITT Cannon Electric Canada
Four Cannon Court
Whitby, Ontario L1N 5V8
CANADA
Attn: B. D. Vallillee

Imatran Voima Oy
Electrotechn. Department
P.O. Box 138
SF-00101 Helsinki 10
FINLAND
Attn: B. Regnell
K. Koskinen

Institute of Radiation Protection
Department of Reactor Safety
P.O. Box 268
00101 Helsinki 10
FINLAND
Attn: L. Reiman

Instituto de Desarrollo y Diseno
Ingar - Santa Fe
Avellaneda 3657
C.C. 34B
3000 Santa Fe
REPUBLICA ARGENTINA
Attn: N. Labath

Japan Atomic Energy Research Institute
Takasaki Radiation Chemistry
Research Establishment
Watanuki-machi
Takasaki, Gunma-ken
JAPAN
Attn: N. Tamura
K. Yoshida

Japan Atomic Energy Research Institute
Tokai-Mura
Naka-Gun
Ibaraki-Ken
319-11
JAPAN
Attn: Y. Koizumi

Japan Atomic Energy Research Institute
Osaka Laboratory for Radiation Chemistry
25-1 Mii-Minami machi,
Neyagawa-shi
Osaka 572
JAPAN
Attn: Y. Nakase

Kraftwerk Union AG
Department R361
Hammerbacherstrasse 12 + 14
D-8524 Erlangen
WEST GERMANY
Attn: I. Terry

Kraftwerk Union AG
Section R541
Postfach: 1240
D-8757 Karlstein
WEST GERMANY
Attn: W. Sieglar

Kraftwerk Union AG
Hammerbacherstrasse 12 + 14
Postfach: 3220
D-8520 Erlangen
WEST GERMANY
Attn: W. Morell

Motor Columbus
Parkstrasse 27
CH-5401
Baden
SWITZERLAND
Attn: H. Fuchs

NOK AG Baden
Beznau Nuclear Power Plant
CH-5312 Doettingen
SWITZERLAND
Attn: O. Tatti

Norsk Kabelfabrik
3000 Drammen
NORWAY
Attn: C. T. Jacobsen

Nuclear Power Engineering Test Center
6-2, Toranomom, 3-Chome
Minato-ku
No. 2 Akiyana Building
Tokyo 105
JAPAN
Attn: S. Maeda

Ontario Hydro
700 University Avenue
Toronto, Ontario M5G 1X6
CANADA
Attn: R. Wong
B. Kukreti

Oy Stromberg Ab
Helsinki Works
Box 118
FI-00101 Helsinki 10
FINLAND
Attn: P. Paloniemi

Rheinisch-Westfallscher
Technischer Uberwachung-Vereln e.V.
Postfach 10 32 61
D-4300 Essen 1
WEST GERMANY
Attn: R. Sartori

Sydskraft
Southern Sweden Power Supply
21701 Malmo
SWEDEN
Attn: O. Grondalen

UKAEA
Materials Development Division
Building 47
AERE Harwell
OXON OX11 0RA
ENGLAND
Attn: D. C. Phillips

United Kingdom Atomic Energy Authority
Safety & Reliability Directorate
Wigshaw Lane
Culcheth
Warrington WA3 4NE
ENGLAND
Attn: M. A. H. G. Alderson

Waseda University
Department of Electrical Engineering
4-1 Ohkubo-3, Shinjuku-ku
Tokyo
JAPAN
Attn: K. Yahagi

1100 F. L. Vook
1120 J. B. Gerardo
1124 A. Owyong/A. V. Smith
1200 G. Yonas
1234 J. Chang/G. J. Lockwood
1800 R. L. Schwoebel
1810 R. G. Kepler
1811 L. A. Harrah
1811 R. L. Clough
1813 J. G. Curro
1813 K. T. Gillen
1815 R. T. Johnson
2155 J. E. Gover
2155 O. M. Stuetzer
2341 M. B. Murphy
5200 W. C. Myre
6200 V. L. Dugan
6300 R. W. Lynch
6336 D. McKeon
6400 A. W. Snyder
6410 A. W. Snyder, Acting
6420 J. V. Walker
6440 D. A. Dahlgren
6441 M. Berman
6442 W. A. Von Rieseemann
6444 S. L. Thompson
6445 B. E. Bader
6445 L. D. Bustard
6445 C. M. Craft
6445 E. A. Salazar
6446 L. L. Bonzon (4)
6446 W. H. Buckalew
6446 J. W. Grossman
6446 D. B. Hente
6446 F. V. Thome
6446 F. J. Wyant
6447 D. L. Berry
6450 J. A. Reuscher
6450A J. Bryson
6452 M. Aker/J. S. Philbin
8214 M. A. Pound
3141 L. J. Erickson (5)
3151 W. L. Garner

